

Benchmarking Spiking Neurons for Linear Quadratic Regulator Control of Multi-linked Pole on a Cart: from Single Neuron to Ensemble

Shreyan Banerjee¹, Luna Gava², Aasifa Rounak¹, Vikram Pakrashi¹

¹ UCD Centre for Mechanics, Dynamical Systems and Risk Laboratory, School of Mechanical and Materials Engineering, University College Dublin, Belfield, Dublin 4, Dublin, Ireland.

² Event-Driven Perception for Robotics, Istituto Italiano di Tecnologia, Via San Quirico 19d, 16163, Genova, Italy.

E-mail: vikram.pakrashi@ucd.ie

March 2024

Abstract. The emerging field of neuromorphic computing for edge control applications poses the need to quantitatively estimate and limit the number of spiking neurons, to reduce network complexity and optimize the number of neurons per core and hence, the chip size, in an application-specific neuromorphic hardware. While rate-encoding for spiking neurons provides a robust way to encode signals with the same number of neurons as an ANN, it often lacks precision. To achieve the desired accuracy, a population of neurons is often needed to encode the complete range of input signals. However, using population encoding immensely increases the total number of neurons required for a particular application, thus increasing the power consumption and on-board resource utilization. A transition from two neurons to a population of neurons for the LQR control of a cartpole is shown in this work. The near-linear behavior of a Leaky-Integrate-and-Fire neuron can be exploited to achieve the Linear Quadratic Regulator (LQR) control of a cartpole system. This has been shown in simulation, followed by a demonstration on a single-neuron hardware, known as Lu.i. The improvement in control performance is then demonstrated by using a population of varying numbers of neurons for similar control in the Nengo Neural Engineering Framework, on CPU and on Intel's Loihi neuromorphic chip. Finally, linear control is demonstrated for four multi-linked pendula on cart systems, using a population of neurons in Nengo, followed by an implementation of the same on Loihi. This study compares LQR control in the NEF using 7 control and 7 neuromorphic performance metrics, followed by a comparison with other conventional spiking and non-spiking controllers.

Keywords: spiking neuron, Lu.i, feedback control, cartpole, multi-linked pendulum on a cart, Nengo, Loihi

1. Introduction

Neuromorphic technology, based on the hardware implementation of spiking neurons and the co-localization of memory and computation, is a promising venue for low-power, low-latency computation on the edge [11]. These properties make neuromorphic a key enabling technology for applications that require fast reactions to sensory stimuli with limited space and power budget. While a lot has been done in the domain of sensing and perception [18], the work on spike-based control is still limited. Among these few works, some were applied to control different robotic platforms using neuromorphic processors [31, 10, 48, 39, 41, 13, 16, 43, 27]. A complete spike-based architecture to control the robot head movements from the dynamic vision sensor in open-loop was presented [31]. Conventional control techniques, such as the Proportional Integral and Derivative (PID) control have been applied to drones using neuromorphic computing [39], where a rate-encoded error signal is passed to populations of spiking neurons corresponding to the P, I, and D coefficients, and the control torque is obtained by summing up the output. This is done on the Loihi neuromorphic chip [10]. Similarly, a closed-loop PID controller for the humanoid robot iCub was presented [48] (using an open-source iCub humanoid platform simulator called iCubSim, controlled with Yet Another Robot Platform (YARP)), which encodes the space-of errors using a space-to-rate encoding scheme and implements the P, I, and D terms using three separate populations of spiking neurons.

DeWolf *et al.* [13] demonstrates the adaptive control of a robotic arm using anatomically structured spiking neurons using the Neural Engineering Framework (NEF). The dynamics of the robotic arm is computed and the target to be reached is provided to the anatomically organized REACH model, that computes the desired joint forces. Volinski *et al.* [16] also uses the REACH model in the NEF framework for adaptive control of a wheelchair-mounted robotic arm for people with upper body disabilities. Ehrlich *et al.* [43] shows that SNNs require much less parameters and inference times compared to ANNs for the estimation of inverse kinematics in robotic systems. The authors used Intel’s Loihi neuromorphic hardware and non-spiking NVIDIA’s Xavier to demonstrate their results on a 6-DOF robotic arm system. The use of NEF to implement PID control on a 3-DOF robotic arm by mapping the PID coefficients on the synaptic weights has also been demonstrated in [27]. DeWolf *et. Al.* [12] implements an SNN running on Intel’s Loihi neuromorphic chip to control a 7-DOF robotic arm in simulation. This work shows that the energy consumption and the computational latency in Loihi is very less compared to standard digital hardware like CPU and GPU. Zaidel *et. Al.* [47] demonstrates inverse kinematics and the PID control of 6-DOF robotic arm using the NEF. Arana *et. Al.* [3] demonstrates the regularization and trajectory tracking of an underactuated Ball and Plate platform using SNNs with NEF. Other studies focused on spiking-based control of canonical and extensively studied mechanical systems, such as the inverted pendulum. This system choice is preferred as a starting point for the control study because it can scale up in complexity by adding

components, such as more links, and can modify behaviour by changing the physical characteristics of the system. Moreover, the cartpole represents an under-actuated system whose control is challenging and its dynamics form the basis of other kinds of systems such as self-balancing robots, human transporters, bipedal locomotion, and missile launching. For example, a moving wheel inverted pendulum (MWIP) system was balanced using a SNN-based linear quadratic regulator (LQR) [25] implemented in the Neural Engineering Framework known as Nengo [7]. This work shows that the control signal is noisy, but it can still reduce steady-state errors for the system response variables over time. At the same time, another study related to the control of canonical mechanical systems [45] addressed both swing-up and stabilization of a double pendulum using an SNN learnt through evolutionary computing, combined with an LQR controller. A benchmark example of using cartpole as a system with multiple levels of difficulty, multiple parameter settings of the RISP neuroprocessor, and multiple spike encoding schemes for applying neuromorphic reinforcement learning (RL) agents have been demonstrated by Plank *et. Al.* [32]. An optimal spike encoding algorithm called SECLOC is devised and used to control a cartpole both in simulation and hardware, using PID and LQR controllers by Diaz *et. Al.* [14]. A closed-loop optimal control using Linear Quadratic Gaussian (LQG) controller on a spring-mass-damper and a cartpole system using Spike Coding Network (SCN) is demonstrated by Slijkhuis *et. Al.* [38]. A cloud edge-based online supervised learning framework is proposed by Ahmadvand *et. Al.* [1], that can work under strict energy constraints. The effect of different decoding schemes and a learned encoding scheme on the evolutionary training of a cartpole and a lunar lander system is explored by Rafe *et. Al.* [35]. This work shows an inverse relationship between the state exposure times and the generations needed to reach the goal for the reinforcement learning agent. An evolutionary framework for training the connectivities in a spiking neural network using a synapse-level Bellman equation is proposed by Banerjee *et. Al.* [5]. An adaptive LQR-based control of a cartpole using Prescribed Error Sensitivity learning rule has been proposed by Banerjee *et. Al.* [4]. Arana *et. Al.* [2] uses a controller designed using the Neural Engineering Framework (NEF) for the stabilization and tracking of an Unmanned Aircraft System (UAS), using PD-like control.

Despite these contributions, existing literature lacks the demonstration of the effect of the number of neurons on vital control performance metrics. Topology evolution methods mostly rely on heuristics [34] and limit their work to a double-pendulum. A significant effort in limiting the number of neurons needed for a control application has been taken by Cook [9], which suggests that only two spiking neurons may suffice for a controller to learn bicycle riding in simulation.

However, there is a need to quantitatively analyze the number of neurons required for controlling more universal canonical systems to ensure scalability and reduce the footprint on neuromorphic hardware to be applied for edge control applications.

The main objective of the paper is to show the variation of control performance metrics and on-board resource utilization, as one moves from rate encoding of the input

with very few neurons, to population encoding, by varying the number of neurons. This is demonstrated using a cartpole as a canonical system. This knowledge is also used to control a multi-linked pendulum on a cart, both in simulation and on hardware. This is important because neuromorphic systems operate within strict constraints on power, and resource utilization. Limiting the number of neurons is of prime importance when deploying neuromorphic chips on the edge, where there is a limited space and energy budget. Various spiking models of neurons have been proposed in the literature, each based on a particular type of biological neuron [30, 24, 28, 36]. In this work, the Leaky-Integrate-and-Fire (LIF) model is employed due to its near-linear behaviour and diverse applications.

Then key contributions of the paper are:

- Demonstrating LQR-based balancing of a cartpole using two LIF neurons, both in simulation and hardware, with a rate-based encoding scheme.
- Moving from rate-based to population-based encoding using an ensemble of spiking neurons in Nengo NEF to increase the precision of control for a cartpole. This is supported by an exploratory analysis of the effect of increasing the number of neurons on the Key Performance Indicators (KPIs) of neuromorphic computing (on CPU and Loihi), and control.
- Using population-encoded neurons to control 1 to 4-linked poles on a moving cart and studying the KPIs thereof.
- Implementing such an ensemble on Intel’s Loihi neuromorphic chip to control 1 to 2-linked poles on a moving cart.
- Comparing this implementation with 3 other spiking controllers and 4 non-spiking controllers, and studying the KPIs for control and neuromorphic simulation thereof.

This study will benefit edge applications of neuromorphic boards by constraining the power requirements, computational overhead, onboard space allocation, and weight. Section 2 explains the control method and the system equations used in designing the simulator. Section 3 outlines the experiments performed, both in simulation and hardware. Section 4 illustrate the outcomes of the experiments and section 5 concludes the study with some future directions.

2. Methods

The inverted pendulum on a cart [17] is a canonical system often used to study linear and non-linear under-actuated control. A cart with a single pole hinged to it, rotating in a plane forms the cartpole. It has two degrees of freedom (DOFs) corresponding to the linear motion of the cart and the rotatory motion of the pole, respectively. Additionally, the study of chaotic dynamics and their control can be performed with multi-linked pendulums on a cart for large angles [26, 21]. Xin et. al. [46] demonstrated that an n-linked pendulum on a cart has linear controllability around its Unstable Equilibrium Position (UEP) for all physical parameters. The subsequent subsection presents the

equations of motion for the chosen system followed by the equations applicable to a general system with an n-linked pendulum on a cart.

2.1. Cartpole Dynamics

Figure 1 shows a schematic of the cartpole system with two state variables, namely, x , which is the displacement of the cart on the rail centered at 0 and θ , which is the angular displacement of the pole about the vertical Unstable Equilibrium Position (UEP). The control objective is to balance the pole for small angle perturbations about the UEP, by applying a positive or negative force F on the cart in one dimension along the rail to move it to the right or the left respectively. The general equations of motion for any system are:

$$\ddot{\mathbf{X}} = f(\mathbf{X}, \mathbf{U}) \quad (1)$$

and its corresponding linearized model is:

$$\begin{cases} \dot{\mathbf{X}} = A\mathbf{X} + B\mathbf{U} \\ \mathbf{Y} = C\mathbf{X} + D\mathbf{U} \end{cases} \quad (2)$$

where X is the system state, U is the control input, and Y is the observable output, A, B, C and D are the system parameter matrices.

For the cartpole, we define the state and the control input as:

$$\mathbf{X} = \begin{bmatrix} x & \dot{x} & \theta & \dot{\theta} \end{bmatrix} \quad (3)$$

$$U = F \quad (4)$$

To get the values of the state parameter matrices A and B , the Lagrangian equations are solved to derive the system-specific equations of motion for the cartpole:

$$\begin{bmatrix} m + M & ml\cos(\theta) \\ m\cos(\theta) & ml \end{bmatrix} \begin{bmatrix} \ddot{x} \\ \ddot{\theta} \end{bmatrix} = \begin{bmatrix} mlsin(\theta)\dot{\theta}^2 + F \\ mgsin(\theta) \end{bmatrix} \quad (5)$$

where g is the acceleration due to gravity, l is the length of the pole, M is the mass of the cart, m is the mass of the pole, and F is the force on the cart.

Using small angle perturbations around the UEP ($\theta = 0$), allows us to substitute $\sin(\theta)$ with θ , and $\cos(\theta)$ with 1, while the squared terms approximate to zero. These approximations give a linearized state-space model of the cartpole:

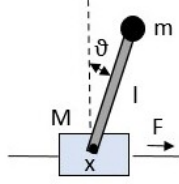


Figure 1: The cartpole system, where x is the position of the cart on the rail, θ is the angle of the pole from the vertical, \vec{F} is the force on the cart, M is the mass of the cart, m is the mass of the pole, and l is the pole length. The other symbols hold their usual meanings.

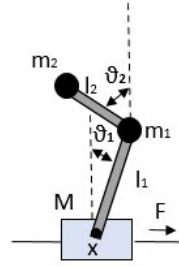


Figure 2: Double inverted pendulum on a cart. α and β are respectively the angles of the first and second links with respect to the vertical(anticlockwise positive).

$$\left\{ \begin{array}{l} \begin{bmatrix} \dot{x} \\ \ddot{x} \\ \dot{\theta} \\ \ddot{\theta} \end{bmatrix} = \begin{bmatrix} 0 & 1 & 0 & 0 \\ 0 & 0 & -\frac{mg}{M} & 0 \\ 0 & 0 & 0 & 1 \\ 0 & 0 & -\frac{(m+M)g}{ml} & 0 \end{bmatrix} \begin{bmatrix} x \\ \dot{x} \\ \theta \\ \dot{\theta} \end{bmatrix} + \begin{bmatrix} 0 \\ \frac{1}{M} \\ 0 \\ -\frac{1}{Ml} \end{bmatrix} u \\ \begin{bmatrix} y_1 \\ y_2 \\ y_3 \\ y_4 \end{bmatrix} = \begin{bmatrix} 1 & 0 & 0 & 0 \\ 0 & 1 & 0 & 0 \\ 0 & 0 & 1 & 0 \\ 0 & 0 & 0 & 1 \end{bmatrix} \begin{bmatrix} x \\ \dot{x} \\ \theta \\ \dot{\theta} \end{bmatrix} \end{array} \right. \quad (6)$$

Extending this analysis to an n -linked pendulum on a cart ($n+1$ DOF) the general equations of motion are obtained:

$$\dot{\mathbf{X}} = A_{n \times n} \mathbf{X}_{n \times 1} + B_{n \times m} \mathbf{U}_{m \times 1} \quad (7)$$

$$\mathbf{Y}_{p \times 1} = C_{p \times n} \mathbf{U}_{n \times 1} \quad (8)$$

The equations of motion for a n -linked pole on a cart has the following form,

$$A\ddot{\mathbf{X}} = B + C \quad (9)$$

where

$$A = \quad (10)$$

$$\begin{bmatrix} \sum_{i=1}^n m_i + M & (\sum_{i=1}^n m_i)l_1 \cos(\theta_1) & \dots & m_n l_n \cos(\theta_n) \\ (\sum_{i=1}^n m_i) \cos(\theta_1) & \ddots & & \\ \vdots & & [a_{ij}] & \\ m_n \cos(\theta_n) & & & \ddots \end{bmatrix} \quad (11)$$

where

$$a_{ij} = \left[\sum_{k=\max(i,j)}^n m_k l_j \cos(\theta_i - \theta_j) \right] \quad (12)$$

$$B = \begin{bmatrix} \sum_{j=1}^n [(\sum_{i=j}^n m_i) l_j \sin(\theta_j) (\dot{\theta}_j)^2] \\ -\sum_{k=1}^n [(\sum_{j=\max(1,k)}^n m_j) l_k (\dot{\theta}_k)^2 \sin(\theta_i - \theta_k)] \\ \vdots \\ -m_n \sum_{k=1}^n [l_k (\dot{\theta}_k)^2 \sin(\theta_i - \theta_k)] \end{bmatrix} \quad (13)$$

$$C = \begin{bmatrix} u \\ (\sum_{k=1}^n m_k) g \sin(\theta_i) \\ \vdots \\ m_n g \sin(\theta_n) \end{bmatrix} \quad (14)$$

Linearizing this model for small angles, the general equations of motion are derived:

$$A_l \ddot{\mathbf{X}} = C_l \quad (15)$$

where

$$A_l = \begin{bmatrix} \sum_{i=1}^n m_i + M & (\sum_{i=1}^n m_i)l_1 & \dots & m_n l_n \\ (\sum_{i=1}^n m_i) & \ddots & & \\ \vdots & & [a_{l_{ij}}] & \\ m_n & & & \ddots \end{bmatrix} \quad (16)$$

where

$$a_{l_{ij}} = \left[\sum_{k=\max(i,j)}^n m_k l_j \right] \quad (17)$$

$$C = \begin{bmatrix} u \\ (\sum_{k=1}^n m_k)g\theta_i \\ \vdots \\ m_n g\theta_n \end{bmatrix} \quad (18)$$

Figure 2 shows a schematic of the such a system with 3 DOFs, called the double inverted pendulum on a cart system.

From the controllability matrix [29], it can be formally proved that these systems are fully controllable [46].

2.2. LQR

We apply linear control using state variable feedback for the cartpole described in Section 2.1. The control objective is to balance the pole for small-angle perturbations about the unstable equilibrium position (UEP), where the system behaves linearly and can be controlled (balanced) with a linear controller. The aim is to bring all the pole angles to 0, considering UEP as the reference for the poles. The chosen controller, known as the Linear Quadratic Regulator (LQR) [23, 44] is preferred to classical Proportional Integral Derivative (PID) controller [37] due to its robustness, superior control performances, and ability to deliver precise control metrics. LQR chooses a set of $m \times n$ state feedback coefficients K for a state vector \mathbf{X} of length n by minimizing a quadratic cost function J :

$$J = \int (\mathbf{X}^T Q \mathbf{X} + \mathbf{U}^T R \mathbf{U}) dt \quad (19)$$

In order to attain the desired transient and steady-state response characteristics for the cartpole, LQR allows for adjusting the values of the state and control cost matrices Q and R , respectively. Elevating the values for the elements in Q increases the speed of response allowing quicker and more aggressive control, while a higher value of R reduces the energy to be spent on the control.

Minimization of the cost function is obtained by solving the Algebraic Riccati Equation (ARE) [37] to obtain the feedback vector $K_{m \times n}$. The control law is given by:

$$\mathbf{U}_{m \times 1} = -K_{m \times n} \cdot \mathbf{X}_{n \times 1} \quad (20)$$

where n is the state vector dimension and m is the dimension of the control input. In the cartpole case, there are four state variables and one control input,i.e., $n = 4$, and $m = 1$.

This control law shows a matrix multiplication to be emulated using spiking neurons.

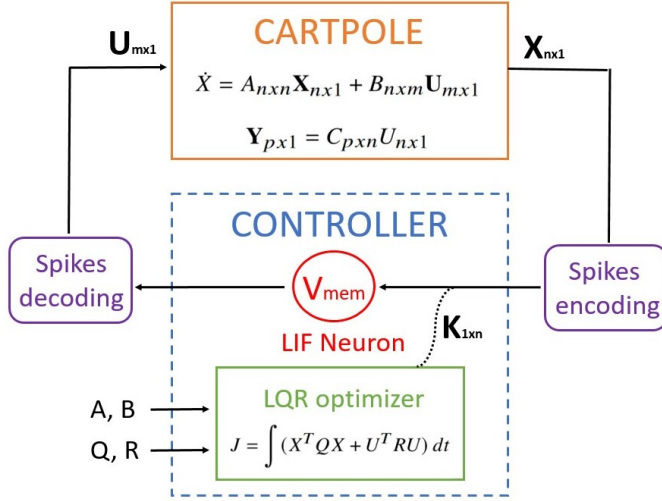


Figure 3: The control pipeline has three two blocks: the CARTPOLE as the system to be balanced, and the CONTROLLER made of the LIF neurons as the computational units and the LQR optimizer as the control method.

2.3. LIF Neuron

A spiking neuron uses a mixed-signal form of computation, with its data encoded as a sequence of spikes. These spikes are spatio-temporally distributed and the information within the signal can be encoded through methods like frequency (rate encoding), population encoding (where a population of neurons encode the entire signal), or latency encoding (precise timing of the spike). Among the many available spiking neuron models, the LIF neuron model was selected, showing that two spiking neurons or a spiking neuron with some pre and post-processing is sufficient for the application at hand. Incoming pre-synaptic spikes Θ are filtered at the synapse to produce an analog synaptic current I_{syn} that induces a change in the membrane potential V_{mem} of the neuron:

$$C_{mem} \frac{dV_{mem}}{dt} = -g_{leak}(V_{mem} - V_{leak}) + I_{syn} \quad (21)$$

where V_{leak} is the leakage voltage, $g_{leak} = \frac{1}{R_{leak}}$ is the synaptic conductance, and C_{mem} is the membrane capacitance.

When V_{mem} crosses a pre-defined threshold V_{th} , the neuron outputs spikes δ :

$$I_{out} = \begin{cases} \delta & \cdots V_{mem} \geq V_{th} \\ 0 & \cdots \text{otherwise} \end{cases} \quad (22)$$

where I_{out} is the output current comprising spikes δ . The rate of change of membrane potential with the synaptic current depends on the membrane time constant $\tau_{mem} = \frac{1}{R_{leak}C_{mem}}$. If a neuron receives spike trains through n synaptic inputs, then the synaptic current [40, 19] at the right-hand-side of Equation 21 at a time instant t is obtained by convolving the input spikes with a synaptic kernel of length τ_{syn} :

$$I_{syn} = \sum_{x=-\infty}^{-\infty} \sum_i^n \Theta(x - t_i) e^{-(\frac{t-x}{\tau_{syn}})} \quad (23)$$

where Θ is the pre-synaptic spike computed as the Heaviside step function:

$$\Theta(t - t_i) = \begin{cases} 1 & \dots t \geq t_i \\ 0 & \dots t < t_i \end{cases} \quad (24)$$

In the simulation environment, Equation 23 can be simplified assuming that τ_{syn} is very high and the synaptic kernel collapses to a summing junction. Considering the duty cycle of Θ to be very small, it converts into a Dirac-Delta function:

$$\delta(t - T) = \begin{cases} I_{spk} & \dots t = T \\ 0 & \dots otherwise \end{cases} \quad (25)$$

where I_{spk} is the amplitude of each spike which is equal to one.

The final simplified version of Equation 23 is shown in Equation 26.

$$I_{syn} = \sum_{t=-\infty}^{\infty} \sum_j^n \delta(t - t_j) \quad (26)$$

where I_{syn} is the synaptic current of the i^{th} neuron receiving spikes through j synaptic inputs, t_j is the time of spike from the j^{th} synaptic input.

2.4. LIF neuron in the cartpole feedback control loop

Figure 3 shows the control system block diagram where the LIF neuron is placed in the feedback control after its weights are tuned to match the K values obtained from the LQR optimizer block (see Equation 20). The states of the system are frequency encoded into spike trains which are then fed to the dendrites of the LIF neuron. The values of the feedback LQR coefficients K are matched with the weights on the dendrites. The spike output received is decoded using a linear decoding scheme by scaling the frequency of the output spike train obtained. As shown in Equations 21 and 23, a noteworthy observation emerges when setting τ_{mem} and τ_{syn} to a very high value. Under these conditions, the membrane potential V_{mem} exhibits a linear relationship with the synaptic current I_{syn} and the synapse behaves like a summing junction. This linearization forms the basis for implementing linear state feedback control with LIF neurons. By adopting this parameter configuration alongside a frequency encoding approach for the spikes, the resulting neuron output frequency becomes approximately proportional to the weighted sum of the input spike frequencies. Table 1 shows the equations for the input-output frequency relationship of a LIF neuron with n synaptic inputs. The output frequency is proportional to the weighted sum of input frequencies. If $K = \frac{I_{mag}}{V_{th}C_{mem}}$ is chosen to be close to unity, then output frequency comes as equal to weighted input frequencies. Hence, a scaled version of the output can be used as the control signal when the input is the state and the weights are set equal to the feedback coefficients.

Table 1: Equations for an LIF neuron with high τ_{mem} and low τ_{syn} . Symbols carry the same meaning as described in Section 2.

Input frequency	Synaptic current	Potential change	Output frequency
$f_i = \frac{1}{T} \sum_{t=1}^T \delta(t - t_i)$ $t_i = \text{input spike timing for the } i^{\text{th}} \text{ neuron}$	$I_{syn} = \frac{1}{T} \sum_t^n w_i \delta(t - t_i)$ $= \sum_i^n w_i \times f_i I_{mag}$	$\Delta V_{mem} = \frac{I_{syn}}{C_{mem}}$	$f_{out} = \frac{\Delta V_{mem}}{V_{th}}$ $= \sum_i^n w_i \times f_i \times \frac{I_{mag}}{V_{th} C_m}$

2.5. Population of LIF neurons for the linear control of a higher DOF mechanical system

To study the effect of using a population of neurons for the feedback control of a higher-order mechanical system, the Neural Engineering Framework (NEF) called Nengo is used, which allows the creation of an ensemble that integrates more than one LIF neuron, for signal representation and processing. The NEF is composed of 3 principles [6], namely, representation (for encoding and decoding time-varying signals), transformation (for applying functions to such signals), and dynamics (for representing dynamical equations using recurrent connections). In this work, the representation principle has only been used. Each neuron in NEF is sensitive to a certain range of positive or negative input currents, known as the receptive field of the neuron. This sensitivity is determined by the tuning curves of the neurons.

From the principle of the NEF, a greater number of neurons per ensemble divides the input space into multiple sub-spaces, increasing precision. However, an excessive number of neurons increases the network complexity, size, and power computation and slows down the computation. Hence, it is important to find a sweet spot for the number of neurons where the signal representation is adequately precise, yet the computational complexity is acceptable. The following subsection discusses the block diagram of the feedback control system designed to balance a multi-linked pendulum on a cart with spiking neurons in the loop, using Nengo.

2.5.1. Control flow design in Nengo In order to design the control system in Nengo, with the neuronal ensemble in the loop, the dynamical equations of the system were implemented in Python and all the states were probed. Figure 4 shows six states (for a double-pendulum on a cart system) being sent to the input of the neuron ensemble after being multiplied by the synaptic weights. The ensemble outputs the control signal, which is fed back to the system. Here, the state values are fed through specific channels to the ensemble of neurons, and the decoder weight on each channel is matched to the corresponding value of the state feedback vector K . Based on the tuning curves of the neurons, each neuron actively spikes for a specific range of inputs. Thus, a collection of spike trains is obtained at the output of the ensemble. The control value is linearly decoded by calculating a weighted sum of the output firing rates of the neurons.

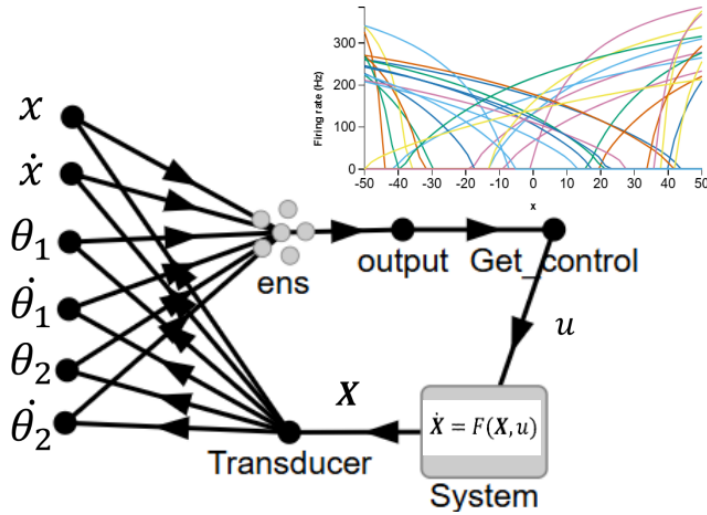


Figure 4: Nengo GUI block diagram for LQR control of a double pendulum on a cart (DPC). The System block represents the DPC simulator that takes in the control signal from the Get_control node and passes the next state to the Transducer. The Transducer sends the six state variables to the nodes which when multiplied by the weights produce the input to the ensemble ens. Based on the tuning curves of the neurons in the ensemble The Get_control node scales the output by -1 to produce the control signal.

3. Experiments on neuromorphic hardwares

Two approaches were chosen for the control of a cartpole: a) Use of fewer neurons for a single pendulum: two neurons were used in simulation and one neuron was deployed in hardware (Section 3.1), and b) Use of an ensemble of spiking neurons for multilinked pendulums (Section 3.2). The neuromorphic control implementation was done using the Loihi chip and the Lu.i board. Both the configurations and descriptions of the neuromorphic boards have been described in detail in the following sections. Section 3.1 first shows a preliminary experiment to test the efficiency of the Lu.i neuron board for a weighted sum of the input operation. Then, Lu.i is used to achieve real-time weighted sum of inputs for the feedback control of a cartpole. Table 2 summarizes the list of experiments conducted: two runs in the CPU using conventional LQR on MATLAB and one using the Lu.i neuromorphic hardware explained in Section 3.1. Section 3.2 first shows an implementation of LQR using an ensemble with a range of neurons from 2 to 2048 neurons in Nengo to balance a pole on a cart, along with various control and neuromorphic performance metrics on the CPU and the Loihi neuromorphic chip. Then a parametric study reflects the effect of varying the ensemble parameters on the control performance. This is followed by the deployment of an ensemble of 100 neurons to achieve feedback control of a multi-linked pendulum on a cart system, backed by an implementation of the same on Loihi. The study concludes with a comparison between various existing models of control using neuromorphic and non-neuromorphic architectures.

3.1. Balancing a pole on a cart using two LIF neurons

Initially, a validation with a simple numerical operation is performed. This is followed by an implementation on a cartpole with an inverted pendulum. The LIF neurons were used to control a cartpole simulator using MATLAB, followed by an experiment with the Lu.i physical board.

3.1.1. Simulations

Cartpole simulator The Cartpole simulator utilizes open-source code by Brunton *et al.* [8], which is useful to define the parameter values and state variables for the system. In contrast to the reference frames specified in the equations of motion in Section 2, the reference angle $\theta = 0$ is defined as the position where the pendulum is hanging vertically downward. Therefore, the control objective is to guide the system to the unstable equilibrium point (UEP), where $\theta = \pi$, starting from small perturbations around this position. During the initial phase of each experiment, the pole is displaced by an angle of 0.2 radians from the UEP. The perturbations applied could be counter-clockwise (positive) and clockwise (negative). Both the cases have been taken into account for the following studies.

Spiking neuron A MATLAB model for a spiking neuron was developed following the Equations 21 and 22. The value of τ_{mem} was set to be very high (100 seconds) following the analysis in the Section 2.3.

LQR setup The LQR feedback coefficients were computed in MATLAB as per the desired response characteristics. The Q and R matrices for this experiment were set to

$$Q = \begin{bmatrix} 1 & 0 & 0 & 0 \\ 0 & 1 & 0 & 0 \\ 0 & 0 & 10 & 0 \\ 0 & 0 & 0 & 10 \end{bmatrix}, R = 0.0001 \quad (27)$$

Cartpole feedback control in simulation The cartpole has four state variables, necessitating the utilization of four synaptic inputs for full control of all the states. Due to the need for both positive and negative control forces, at least two neurons, one firing for positive synaptic inputs and the other one for negative inputs are needed for the simulations. Thus, the first simulation involves using two neurons with 4 dendrites each. One neuron spikes for a positive synaptic current and the other, for a negative synaptic current.

As described above, corresponding to each state variable, four synaptic inputs to a neuron are necessary. However, there is a physical constraint of three inputs on the Lu.i board. To employ Lu.i for control, the information about the state x may be omitted,

Table 2: List of the experiments for cartpole balancing using one or two neurons.

Hardware/ Simulation	Controller	Number of neurons	Inputs per neuron	Controlled States
1 Simulation	MATLAB LIF	2	4	x, θ
2 Simulation	MATLAB LIF	2	3	θ
3 Hardware	Lu.i	1	3	θ

as indicated in Equation 6, where the other states are independent of x . Consequently, only one neuron with three synaptic inputs is used to control the angle of the pole. Thus, the second simulation uses two neurons with 3 dendrites each, for controlling the angle θ of the pole on the cart, without considering the cart position x . The data input to the dendrites were encoded using rate-based encoding, where the frequency of the spikes is proportional to the value of the state variable.

3.1.2. Hardware

Lu.i neuron Lu.i is an educational neuron board [19, 40], developed by the Kirchhoff Institute for Physics, Heidelberg University, Germany. It is based on the LIF model of a spiking neuron and each Printed Circuit Board (PCB) has three synaptic inputs (see Fig. 5a). Details about the schematics and the components can be found at [40] and the relevant features for our work have been summarized in Table 3. Each input has a switch to toggle between positive and negative dendritic weights.

Testing Lu.i for Weighted summation operation A preliminary experiment was performed to assess the efficacy of using Lu.i for multiplying two decimal numbers. One of these numbers is a variable, in this case the spike-encoded state variables, and is taken as an input through the dendrite, and the second number is a constant corresponding to the weight on the dendrite. The purpose of this verification is to evaluate the percentage error and performance before its application as a feedback multiplier for control. The Lu.i neuron was interfaced with a laptop using a Digilent Analog Discovery 2. The oscilloscope and function generator options were used from this data acquisition system [15, 20]. The setup is shown in Figure 5. The output frequency of spikes from Lu.i should ideally be equal to the scalar product of the frequency of the pulse wave provided at the input and the weight assigned to that synaptic input. The power consumed by the Lu.i board was measured from the voltage across its battery and the current drawn by the PCB from the battery, monitored by a series ammeter. The weight on the Lu.i board dendrite (R_w), equivalent to the potentiometer's resistance as mentioned in Table 3, was estimated at 10 Hz input, by measuring the output frequency f_{out} and assuming that

Table 3: Features of interest of the Lu.i neuron board.

Parameters	Number	Description
Synaptic inputs	3	Positive/negative
Tunable parameters	6 potentiometers	3 weights + synaptic time constant + membrane time constant + leakage voltage
Data type	Spikes	Spatio-temporal voltage/ current spikes
Power source	3 volts DC	Battery
Active components	15	7 OpAMPs + 8 MOSFETs
Passive components	27	12 resistors + 6 potentiometers + 2 capacitors + 7 LEDs

the resistance $R_w = \frac{f_{out}}{10}$.

Testing Lu.i as a feedback controller For testing Lu.i for feedback control, an Arduino UNO connected to a laptop running the MATLAB cartpole simulator was used to send and receive a spike train with the desired frequency in real-time (see Figure 5c). The weight potentiometers were tuned based on the calculated values of the LQR feedback coefficients K . The tuning was done within the limits of human error by providing square wave pulses to the three inputs with a certain time delay between themselves and recording the change in the membrane potential (since $\Delta V_{mem} \propto I \times R_w$).

In simulations, a minimum of two neurons was necessary for balancing the pole on a cart. In order to perform the same task using a single neuron in hardware, it requires some pre-processing and post-processing. The implementation was done following the steps below:

- (i) The potentiometers of the Lu.i board were tuned manually to match the approximate ratio given by the MATLAB Riccati Equation Solver. This ensures successful control even though the desired values of the performance metrics may not be achieved.
- (ii) The cartpole was simulated in steps of 5ms (simulation time) laps. Within the span of each time step, the force on the cart remained constant.
- (iii) This control was calculated by computing the sum of spikes for 0.5 seconds (real-time). Thus the Lu.i board provided 2 inferences per second.
- (iv) The input to the dendrites was biased to yield only positive values. This is because for a negative value of synaptic current, the Lu.i board does not return a spike. Thus a positive bias has been provided to the input signal. This input was then

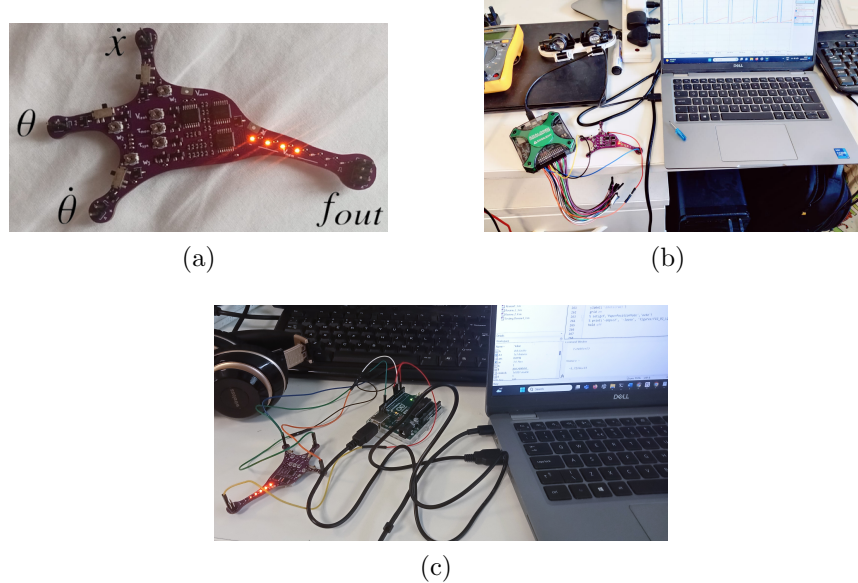


Figure 5: Experimental setup for Lu.i. (a) shows the Lu.i board with the inputs and output labeled, (b) shows the Lu.i board attached to a Digilent DAQ connected to the laptop running the multiplier experiment, (c) shows Lu.i as a controller connected to a laptop running the control algorithm on a cartpole simulator, via an Arduino Uno.

multiplied with 10 kHz to yield an input spike frequency proportional to the value of the state variable.

- (v) Since a single Lu.i neuron was being used, the sign of the post-synaptic current was pre-calculated using the formula $o = kx$. The input spikes were then multiplied by the sign to ensure a positive post-synaptic current, summed over all time steps. These spikes were then sent to the Arduino board via USB.
- (vi) The Arduino UNO sent the spikes to Lu.i via 3 pins and the spikes generated at the axon were received by the Arduino via 1 pin from the Digital Pin Set.
- (vii) Arduino computed the sum of spikes for 0.5s. This value (proportional to the spike output frequency) was sent back to Matlab via USB, which was then multiplied by the sign of o previously computed, to get $o' \propto kx$. This was further scaled/linearly decoded and multiplied with -1 to get the control force $F \approx -kx$. The scaling was done via trial and error to obtain the desired value of the control force.

A point to be noted here is that this weighted-summation operation can also be performed at the input connections of a non-spiking neuron. However, the focus is to verify whether the spiking version can perform this disjunctive sum operation, with an acceptable accuracy for the given control task, provided that the input is rate encoded into spikes. The idea is that, if, by using nearly the same number of spiking neurons as non-spiking ones, a near-optimal control is achievable, then it can be argued (either from the datasheet or from physical measurements) that the power demand of a spiking hardware would be orders of magnitude less than the conventional neural networks for

the target application, at the cost of some computational accuracy.

3.2. Linear control using spiking neuron ensembles

From the previous section, it is seen that two neurons, or a single neuron with some off-chip processing, can perform LQR control of a cartpole, through rate-based encoding scheme. However, for more precise control and to get the desired control performance, a population of neurons, where each neuron spikes for a certain range of control values, is desirable. This is called population encoding scheme [7]. In this work, Nengo Neural Engineering Framework(NEF) based on Python, is used to simulate such populations of neurons. First, an experiment was performed with a cartpole using 2 to 2048 neurons, showing the variation in control and neuromorphic performance metrics. Based on the obtained insights, an ensemble with 100 neurons is chosen to control multi-linked pendulums on a cart, both on simulations and on the Loihi neuromorphic hardware.

3.2.1. Simulations

CPU Specifications : These simulations were run using a Python IDE, running on a 64 bit Ubuntu 22.04.4 LTS OS in a machine with an Intel® Core™ i7-8700K CPU @ 3.70GHz × 12, with a 32 GB RAM.

Balancing a pole on a cart using varying numbers of neurons in the NEF
In this set of experiments, the balancing of a pole on a cart is studied using 2 spiking LIF neurons, using the NEF. While using 2 neurons, the ensemble behaves similar to rate-based encoding, with each neuron spiking for either positive or negative inputs with a frequency proportional to the input value. Then the number of neurons is varied up to 2048, in powers of 2, in order to monitor the variation of control performances, as well as power consumption and on-chip area utilization, besides other neuromorphic metrics. This is followed by a parametric study in which the parameters of the spiking neuron ensemble are varied and the effects on the control performance are studied.

Validating control performance of a multi-linked pendulum on a cart with a 100 neuron ensemble Based on the insights gained, a validation study employing a fixed number of neurons in the ensemble is conducted for the feedback control of a cart-mounted multi-link pendulum system, with configurations ranging from one to four pendulum links. Table 4 lists the experiments carried out in simulations and hardware, the corresponding system configurations and initial conditions. Nengo NEF [11] is used to run the control algorithm, while the system to be controlled is designed in Python with the Lagrangian equations and Runge-Kutta 4th order solver. Here, $\theta = 0$ corresponds to the unstable equilibrium position (UEP) as described in the equations. The number of connections going into the neuron ensemble in Figure 4 depends on the dimension of the state vector. For example, for a cartpole, four inputs are needed, and for a double

Table 4: List of LQR control experiments using Nengo SNNs. Different systems with various characteristics were tested. DPC stands for double pendulum on a cart, TPC for triple pendulum on a cart and 4lPC for 4 linked pendulum on a cart.

	System	DOFs (n)	Perturbation (rad)	Neurons	Synapses	Bob mass (kg)	Pole length (m)	Software /Hardware
1	Cartpole	2	0.2	100	4	1	2	Nengo + Loihi
2	DPC	3	{0.2, 0.18}	100	6	0.5	1	Nengo + Loihi
3	TPC	4	{0.2, 0.18, 0.16}	100	8	1/3	2/3	Nengo
5	4lPC	5	{0.2, 0.18, 0.16, 0.14}	100	10	0.25	0.5	Nengo

pendulum on a cart, six are needed. The weights on the connections are the elements of the feedback coefficient $K_{1 \times 6}$. The control energy tuning parameter R is chosen to be equal to 20, and the state variable tuning parameter Q is chosen such that the coefficients for the angles are 10^4 and for the angular velocities are 10^3 .

This exploratory analysis informs the trade-off to be made between the control performance desired and the number of neurons needed in the ensemble population. Having an approximate knowledge of the least number of neurons that can perform a specific control task reduces the resource utilization, power consumption, on-chip space allocation, and computational burden.

3.2.2. Hardware The experiment with a multi-linked pendulum on a cart system were implemented on Intel’s Loihi neuromorphic hardware, using the Nengo-Loihi backend, and the performance metrics were recorded. Loihi was fabricated using Intel’s $14 - nm$ FinFET process, incorporating 2.07 billion transistors and 33 MB of SRAM across its 128 neuromorphic cores and three x86 cores, all within a die area of 60 mm^2 . The chip operates across a supply voltage range of 0.50 V to 1.25 V. The chip includes 16 MB of synaptic memory. Using its most compact 1-bit synapse representation, Loihi achieves a synaptic density of 2.1 million unique variables per mm^2 . Loihi’s peak neuron density is 2,184 neurons per mm^2 . Table 4 captures the experiments performed on Loihi.

4. Results

The results from the experiments conducted as described in Tables 2 and 4 are presented in the same order as the experiments described in Section 3.

4.1. Balancing of a cartpole using 2 LIF neurons

4.1.1. Simulations Figure 6 (a) shows the state variables x and θ over time for positive and negative perturbations around UEP, using two simulated LIF neurons and four synaptic inputs that receive the cartpole state. Figure 6 (c) shows the evolution of θ

Table 5: Control performance metrics for the pole angle during the control of a cartpole using 2 neurons and 4 dendrites and 2 neurons and 3 dendrites in MATLAB simulation, and with the Lu.i single neuron board. The averages are calculated by using the absolute values for the positive and negative perturbations.

Metrics	2 Neurons 4 Synapses			2 Neurons 3 Synapses			Lu.i		
	Positive	Negative	Average	Positive	Negative	Average	Positive	Negative	Average
T_r (s)	0.13	0.68	0.141	0.11	0.11	0.11	1.76	2.11	1.94
PO	0.4	0.05	0.22	0.1	0.8	0.45	0.35	0.25	0.30
T_s (s)	1.25	4.8	3.03	0.465	1.89	1.77	14.52	14.56	14.54
SSE	≈ 0	≈ 0	≈ 0	-0.0025	-0.0025	0.0025	0.05	-0.05	0.05

over time for positive and negative perturbations around UEP, using two simulated LIF neurons and three synaptic inputs that receive the cartpole states except for the cart position x . The blue segments in Figure 6 (b), (d) depict the spike patterns an the red line corresponds to the control values input to the system to keep it around the UEP. The spike rasters have been divided into segments for enhanced visibility. On zooming into the plots, it can be seen that the spike density is high when the control value is high, and decreases as the control force diminishes, as expected for linear frequency-based decoding scheme.

Table 5 shows a comparative study of the metrics obtained from the two experiments. To analyse the performance, rise time T_r and overshoot (PO) are chosen as the transient characteristics, and steady-state error (SSE) and settling time T_s (time taken to reach a variation of less than 5% about the UEP) as the steady-state characteristics as in [29]. Lower values of these metrics indicate superior control. The main difference between the two simulations is that, for the control with 2 neurons and 3 dendrites, the state information is omitted, hence only the pole angle θ is controlled and not the cart position x . However, control time metrics like T_r and T_s are superior for the 3-dendrite case since only one state variable is controlled.

Please note that the spike density increases with an increase in the control value and gets rarefied as the control value reduces. It is not expected that the control performance will change based on the number of dendrites, because the reduction in dendrites reduces the system state input to the neuron, and hence, the number of system states controlled. In this work, for the 3 dendrite neuron, the information about the cart position x is eliminated, so position control is not possible in this case. Since, for the 3 dendrite situation, only one variable needs to be controlled, the performance metrics are observed to be slightly better than the 4 dendrite case.

4.1.2. Hardware

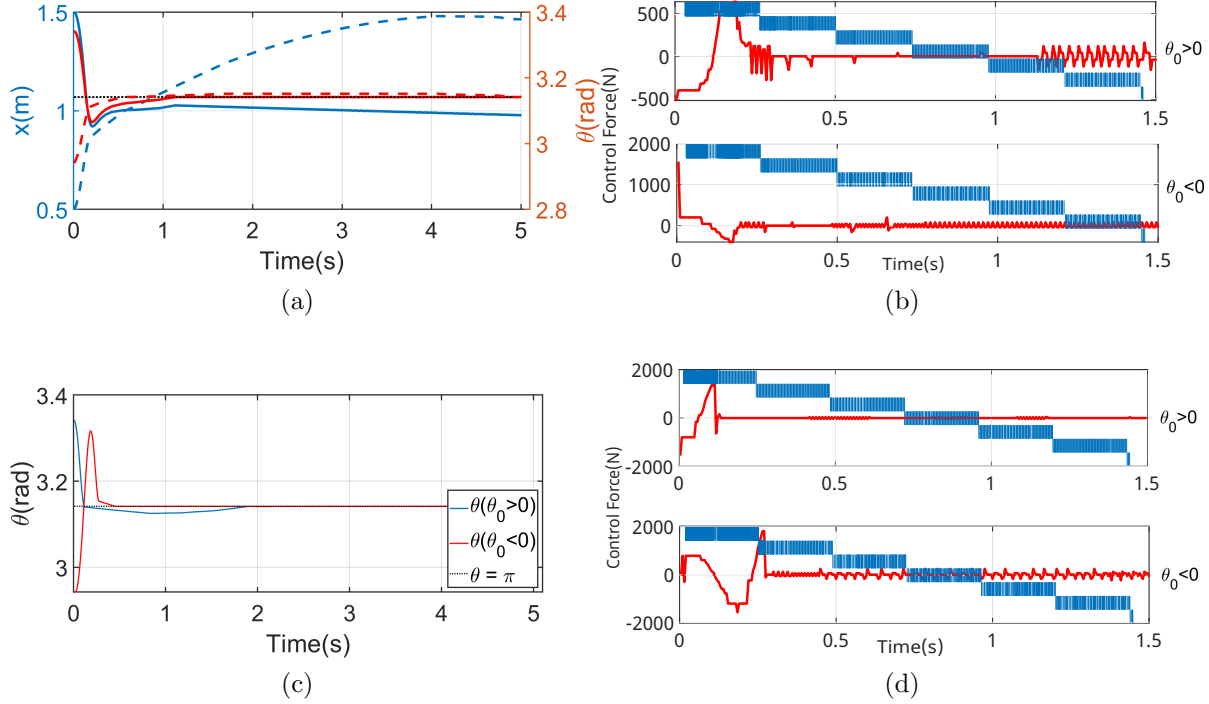


Figure 6: Plots for balancing a cartpole using 2 MATLAB simulated neurons with 4 and 3 dendrites. (a) and (c) show the pole angle evolution for positive and negative initial angles of the pole for 4 and 3 dendrites respectively, while (b) and (d) show the control values and the spike output frequency for the respective cases.

Testing Lu.i as multiplier In order to determine its suitability for being used as a feedback controller, Lu.i was tested for weighted sum of inputs. It was observed that the board consumes a total of around 35mW of power for a 10Hz input frequency.

During the testing, waveforms were recorded with the Digilent scope, and one such visualization of the signals for a 10 Hz input pulse wave and multiplier weight of 1.42 is shown in Figure 7. Figure 7(a) shows the input voltage pulses in orange, and the output voltage pulses in blue. Figure 7(b) shows the membrane potential of Lu.i in orange, and the output voltage pulses in blue. It can be observed in Figure 7(a) that the frequency of the output signal is about 1.47 times the input, which is in close agreement with the expected value of 1.42.

Figure 8 shows Lu.i output has a linear trend when varying the input frequency considering a synaptic weight multiplier of 0.496. A pulse wave was fed at the input with a duty cycle proportional to the frequency. Therefore, the total duration of *high* state of the pulse wave per second is proportional to the input frequency, and consequently the power input to the circuit. Eight samples of input frequency were tested from 5 to 40 Hz. If the duration of each pulse (*high* state) is kept constant, and the frequency is increased, then the duty cycle of the wave increases moving from an approximate spike train to a DC signal. Since an LIF neuron acts as an integrator, the rate of change

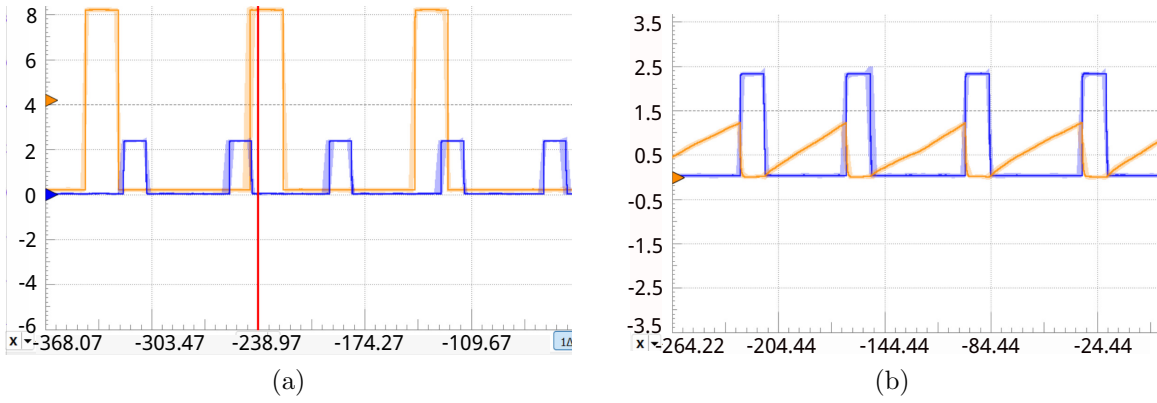


Figure 7: Snapshots of oscilloscope window for multiplication using Lu.i. (a) Input spikes in orange (Channel 1) and the output spikes in blue (Channel 2). X-axis: major div = 64.6 ms/div; Y-axis: major div = 2V/div. (b) Membrane potential and output spikes in channels 1 and 2 respectively. X-axis: major div = 60.0 ms/div; Y-axis: major div = 1V/div.

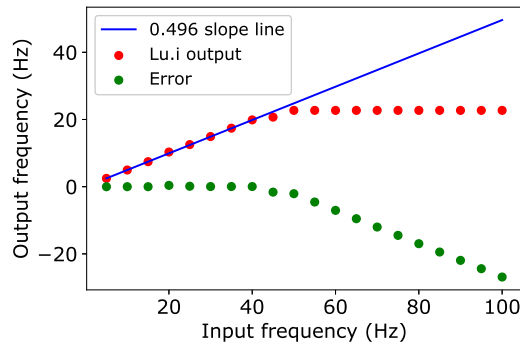


Figure 8: Linear behaviour of the Lu.i output with the input frequency.

Table 6: Results for the experiment of using Lu.i as a multiplier. Two observations are recorded by varying the synaptic weight value for proof of concept and recording the power consumption.

Input(Hz)	Weight	Output(Hz)	Expected (Hz)	Error(%)	Power(mW)
10	1.42	14.73	14.248	3.46	34.31
10	0.71	7.39	7.120	3.81	35.13

of membrane potential, and hence the output spiking frequency depends on the RMS value of the input voltage. Hence, once the input duty cycle becomes sufficiently large, the output frequency saturates. Figure 8 shows such an example for a pulse duration of 20 ms.

The obtained results yield two insightful observations. Firstly, the multiplication error is $\leq 4\%$, a value acceptable for feedback control applications. This is because the feedback multipliers are chosen based on the desired response of the system, both in terms of error and control energy spent. Slight variations in operands and hence the output hold no significant concerns in this context as the primary objective is only to stabilize the pole in its UEP without strict constraints on the response characteristics such as settling time, overshoot, or control energy. Previous works on CMOS-based analog multiplier circuits [42, 33] show an acceptable linearity error range of $< 1\%$ to 2%. This combined with the synaptic non-linearity, membrane non-linearity of the neuron, and target application makes $\leq 4\%$ an acceptable error for this work. Secondly, temporal encoding of the data allows for the same hardware to be used to process a diverse range of inputs if the spike duty cycle can be appropriately chosen to push the saturation effect to a higher frequency range. This contrasts with digital circuits, where the number of components needed increases with the number of operand bits, leading to a strict constraint on the range of data permitted. Thus neuromorphic hardware can be much more scalable compared to non-neuromorphic digital chips. A representative data of the power consumption of the Lu.i board is given in Table 6. Since the number of synaptic operations depends on the input frequency, the power consumption should ideally be the same for the same input frequency as seen from the table.

Testing Lu.i as feedback controller Figure 9 shows the evolution of pole angle θ , the spike output frequency (which is proportional to the control force F), and the spike rasters with time, for both positive and negative starting angles. It is clear that the control is successful, i.e., the pole is successfully steered towards the UEP, starting from the initial position.

Table 5 shows the control performance metrics with the Lu.i board. The experiment shows that the convergence occurs in reasonable time demonstrating that a single spiking neuron or two spiking neurons can be used for LQR control. The metrics reflect that for the implementation on a spiking hardware, the control performance is poorer compared to simulations. The time metrics are much larger for Lu.i which is expected due to the following reasons:

- Spiking hardware provides poorer accuracy and high noise levels (which is not considered in simulations).
- The hardware implementation uses a single neuron to approximate excitatory and inhibitory behaviours, limiting its performance.
- Real-time rate encoding for the hardware is less precise than in MATLAB.
- The communication overhead between Lu.i, Arduino, and the laptop is substantial compared to running everything in a single MATLAB simulation.

After the 15s simulation time, θ is seen to have small oscillations about $\theta = \pi$, within the limits of the steady-state error. Although 2 neurons with a rate-based encoding can control systems with linear state variable feedback type control, unlike a non-spiking

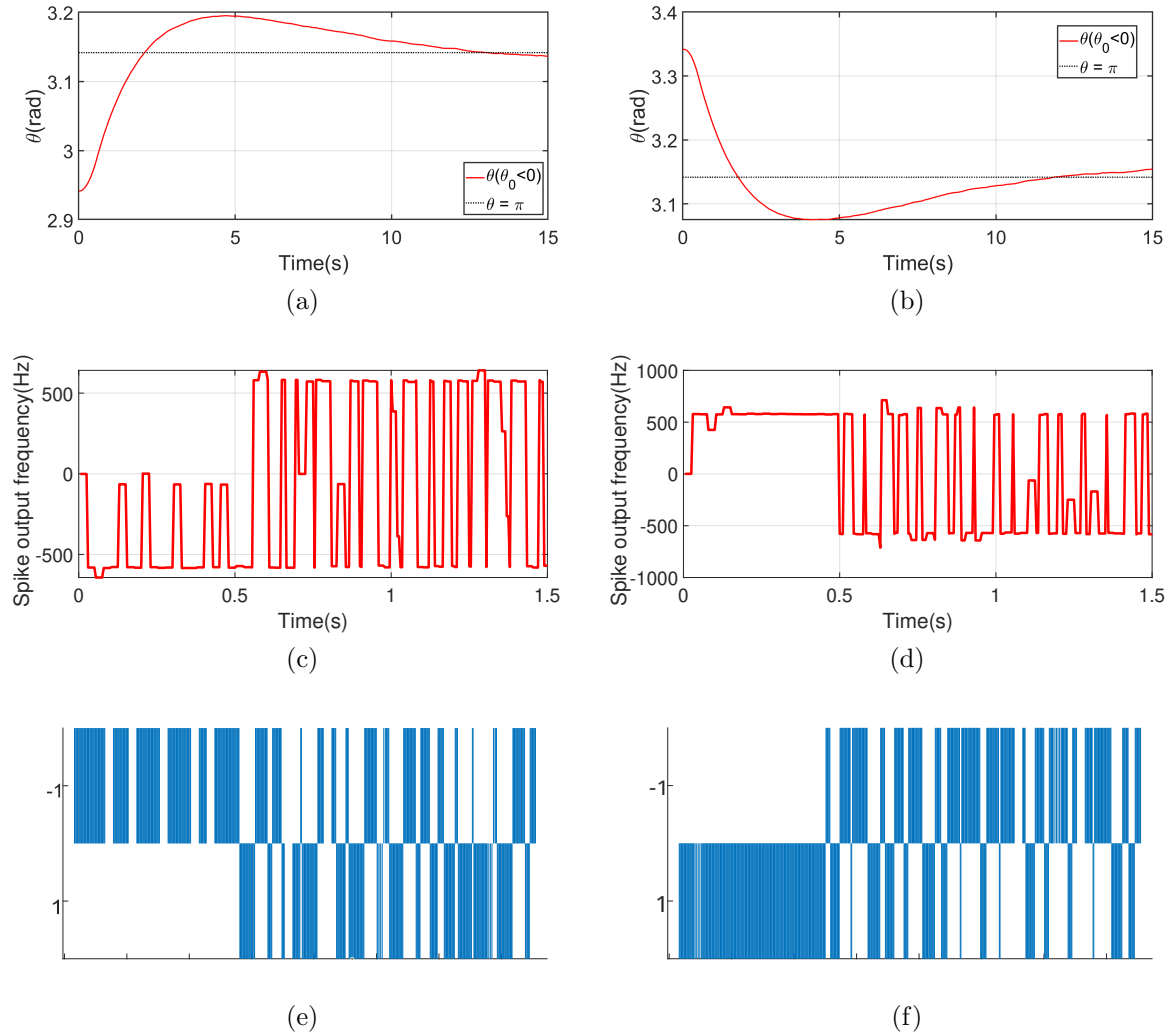


Figure 9: Plots for balancing a cartpole using the Lu.i analog neuron board. The left column shows the plots for the negative initial angle. The right column shows the plots for a positive initial angle. From top to bottom, the rows show the angle evolution over time, the spike output frequency, and the spike raster plot respectively. The control value is a negative scaled version of the spike output frequency.

neuron, to achieve precise end-to-end control with spiking neurons, the number of such neurons needed would be dependent on characteristics such as range and frequency components of the signal to be represented. Hence a population of neurons, each sensitive to a certain range of control values, is needed for precise control, as discussed in the next set of experiments.

4.2. Rate to Population Encoding for Neurons to Balance a Cartpole

From the previous section, it is seen that 2 neurons can adequately balance a pole on a cart system. Although rate-based encoding using a single neuron can achieve linear state

variable feedback control (steer the pole on the cart to the UEP starting from the initial perturbed state) and is robust to noise coming from the fluctuations of the parameters of the board/chip or from encoding imperfections (i.e., when the spike encoding of the state or the values of current generated by the neurons, vary within a small interval between successive trials, the deviations in the metrics of control don't exceed a certain threshold), it is not very precise (we cannot achieve minor changes in KPIs). To address this, population-based encoding for control is preferred. Here, each neuron encodes a small percentage of the signal, increasing the overall precision. This is because each neuron is sensitive to a small fragment of the signal, and hence collectively, an ensemble of neurons can better represent the entire signal. Here, the Neural Engineering Framework is used for simulating populations of neurons. Although population encoding requires more on-board resources (number of neurons and synapses), it is useful when the precision is more important than the resource/energy constraints.

4.2.1. *Simulation*

Balancing a cartpole with a varying number of neurons in the NEF In this section, the results for controlling a cartpole using an ensemble of neurons in NEF, and the change in control and neuromorphic performance metrics with the number of neurons, are presented. Figure 10 shows the tuning curve for a 2-neuron ensemble in Nengo, used to control a cartpole. From this figure, it is seen that one neuron fires mostly for positive inputs and the other for negative inputs. Clearly, this behavior resembles rate-based encoding, similar to 2-neuron control in MATLAB discussed before. Figure 11 shows the evolution of x and θ for balancing a pole on a cart with 2 neurons for both positive and negative initial angles, and the corresponding filtered control signals and spike raster plots. Now, the number of neurons is increased in powers of 2 from 2 to 2048, and the change in control performance is tabularized in Table 7. The same has been graphically illustrated in Figure 12. A few neuromorphic metrics for the simulation on CPU are highlighted in Table 8, and the energy and resource-utilization for the implementation of such control on the Loihi neuromorphic chip are highlighted in Table 9. It is seen that the control performance improves up to around 128 neurons and then saturates. The IAE (Integral of Absolute Error) and ITAE (Integral of Time-weighted Absolute Error) metrics show a minimum at around 10 neurons and then saturate. Clearly, the neuron requirement is around 100 or even less for the smooth control signal profile needed for balancing a cartpole. From Figure 13 it is seen that the peak allocated memory increases with an increase in number of neurons, although the wall-time remains more or less constant. Also, as expected, the energy and on-board resources (neuron area on chip) keep increasing with the number of neurons as seen in Figure 14. The theoretical energy and chip area are calculated from the unit values provided in the paper on Intel's Loihi neuromorphic board [10]. An important point to note here is that, for the simulations, there are 1000 inferences per second, so for a duration of 10s, the number of inferences is 10^4 . Thus, for a 128 neuron ensemble, the

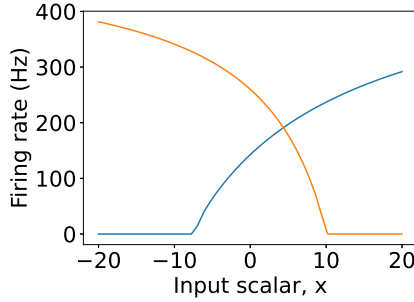


Figure 10: Tuning curves for 2 neuron control in Nengo for positive starting angle of the pole.

Loihi energy consumption is 3 orders of magnitude less than CPU which decreases upto 5 orders of magnitude for a 2 neuron ensemble. The theoretical chip area is compared with the actual chip area requirement by experimentally determining the percentage of neuromorphic cores utilized for the job run. It is seen that though the experimental chip area requirement is slightly less than the theoretical one, both increase comparably with an increase in the number of neurons. Therefore, to limit resource utilization and to design ASICs for a particular application on the edge, a suitable number of neurons needs to be chosen for a particular control problem. Figure 15 shows the control force and spike raster plots for control with 4, 8, 16, and 32 neurons. Two important observations emerge from these plots:

- (i) The noise levels in the control signals decrease with an increase in the number of neurons, as expected. This increases the precision in control.
- (ii) As the number of neurons increases, certain neurons spike, while others remain dormant as seen from the spike raster plots. This is the reason behind the saturation of control performance after a certain point, since the number of neurons actively spiking gets fixed.
- (iii) Although the control performance saturates after around 100 neurons, the peak memory allocation on CPU and the percentage core allocation on Loihi increase drastically. This creates a need to limit the number of neurons needed for the application at hand without compromising with the control performance.

Effects of Variation of NEF Parameters on the Control Performance
 Besides the number of neurons in an ensemble, other parameters like the encoders, intercepts of the tuning curves, and maximum firing rates can be varied to check the effects on the control performance. In this capacity, this section talks about manually altering the tuning curves of a neural ensemble and recording the changes in the control performances thereof.

The intercepts are chosen in three different ways. First they are equally spaced (linear spacing) within a varying interval (Table 10), then a normal distribution is

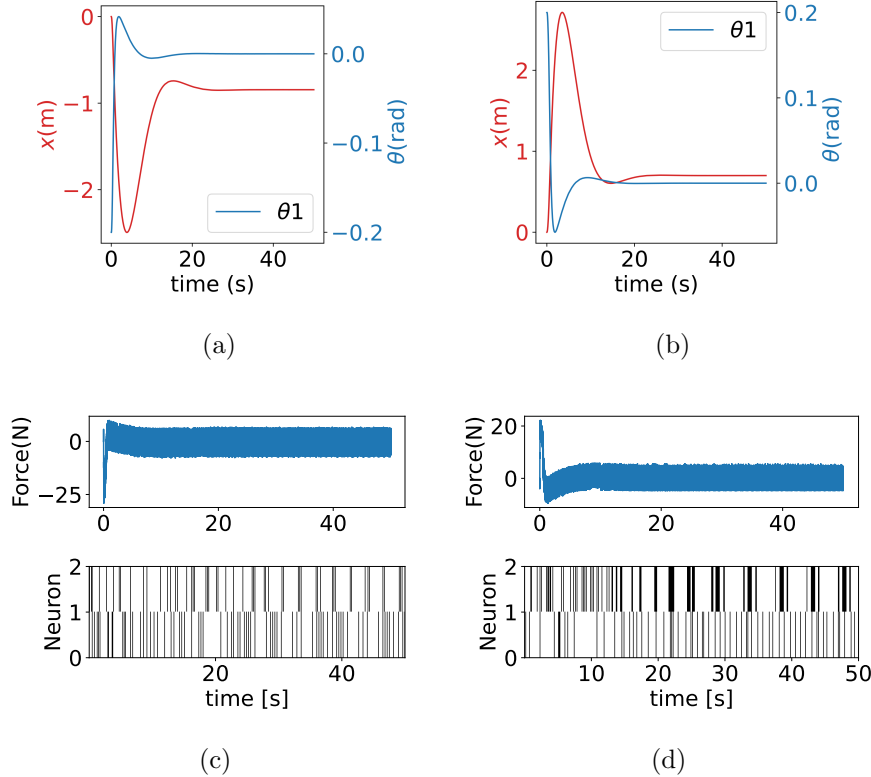


Figure 11: Plots for balancing a cartpole using 2 neurons in the NEF.(a) and (b) show pole angle and cart position evolution over time for positive and negative initial values respectively. (c) and (d) show the corresponding control value and spike pattern.

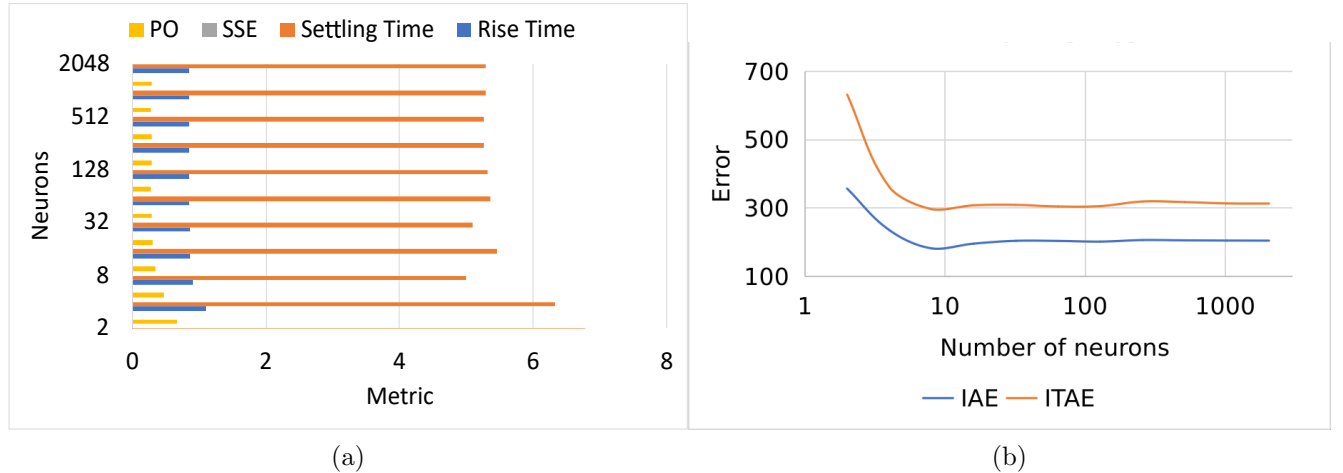


Figure 12: Change of control metric values with the number of neurons for a cartpole.

chosen with mean at 0, and varying standard deviation (Table 11), and finally, the intercepts are sampled from an uniform distribution within a varying interval (Table 12), for a 100 neuron ensemble.

From the tables, it is seen that most of the metrics show a high value for intercepts

Table 7: Control performance of a cartpole for varying numbers of neurons.

Neurons	P.O. (%)	T_r (s)	T_s (s)	SSE ($\times 10^{-5}$)	IAE (rad.s) ($\times 10^{-3}$)	ITAE rad.s ² ($\times 10^{-3}$)	ISC ($N^2 \cdot s$) ($\times 10^2$)
2	67.5	1.483	6.778	226	357.289	632.429	5.74
4	46.8	1.104	6.320	315	235.768	362.054	3.05
8	35.1	0.906	4.994	265	182.391	297.242	24.7
16	30.6	0.863	5.454	27.8	196.206	308.334	2.40
32	29.7	0.863	5.093	63.3	204.459	309.658	2.11
64	29.7	0.856	5.365	34.0	204.155	304.939	2.06
128	28.4	0.857	5.323	3.77	202.119	306.029	2.01
256	28.5	0.857	5.267	22.3	206.671	319.478	2.01
512	28.2	0.854	5.262	28.0	205.808	317.848	1.99
1024	28.4	0.856	5.293	11.8	205.257	313.961	1.99
2048	28.4	0.857	5.283	0.267	205.009	313.597	1.99

Table 8: Neuromorphic performance metrics across different neuron counts on CPU.

Neurons	Sim time (s)	Wall time (s)	Real time factor	Max memory RSS (MiB)	Peak allocated (MiB)	Spikes/neuron ($\times 10^5$)	Estimated CPU energy (J)
2	10.000	18.417	0.543	340.398	4.665	5.975	2.739
4	10.000	18.944	0.528	882.414	4.996	9.590	1.597
8	10.000	19.488	0.513	890.055	5.585	11.886	3.352
16	10.000	18.486	0.541	897.070	6.805	7.422	3.585
32	10.000	20.459	0.488	901.821	9.264	6.815	5.345
64	10.000	18.700	0.535	905.172	14.161	10.406	4.395
128	10.000	18.708	0.534	919.140	23.906	8.376	6.058
256	10.000	19.113	0.523	961.339	43.460	8.831	5.984
512	10.000	19.776	0.507	987.973	82.568	8.206	1.329
1024	10.000	19.052	0.525	1098.559	160.778	8.537	2.109
2048	10.000	21.079	0.474	1317.242	323.659	8.795	3.334

placed very closely about the origin, and saturates to a lower value as the intercepts are spread out in the interval between -1 and 1 . This is because, for extremely low values of intercepts, every neuron fires for the entire range of input data, which reduces the precision of control. Spacing them out causes some neurons to fire for a smaller range of inputs with much higher precision. However, beyond a certain spacing, the

Table 9: Loihi neuromorphic ore utilization and area metrics for increasing neuron counts.

Neurons	Core Utilization (%)	Number of Cores	Experimental Area on chip (mm^2)	Theoretical Area on chip (mm^2)	Estimated Energy ($\mu J/inf$)
2	0.20	1	8.20×10^{-4}	9.00×10^{-4}	9.14×10^{-3}
4	0.40	1	1.64×10^{-3}	1.80×10^{-3}	1.08×10^{-2}
8	0.80	1	3.28×10^{-3}	3.70×10^{-3}	1.96×10^{-2}
16	1.60	1	6.56×10^{-3}	7.30×10^{-3}	2.88×10^{-2}
32	3.10	1	1.27×10^{-2}	1.46×10^{-2}	6.60×10^{-2}
64	6.20	1	2.54×10^{-2}	2.93×10^{-2}	1.56×10^{-1}
128	12.50	1	5.13×10^{-2}	5.86×10^{-2}	2.95×10^{-1}
256	25.0	1	1.03×10^{-1}	1.17×10^{-1}	6.60×10^{-1}
512	50.0	1	2.05×10^{-1}	2.34×10^{-1}	1.26
1024	100.0	1	4.10×10^{-1}	4.69×10^{-1}	2.52
2048	100.0	2	8.20×10^{-1}	9.38×10^{-1}	4.96

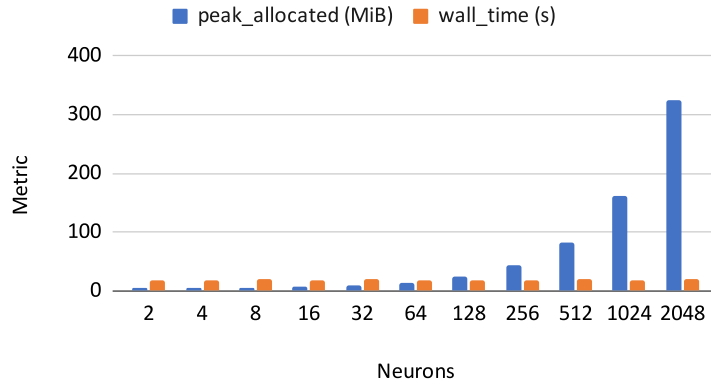


Figure 13: Change of neuromorphic metrics with the number of neurons for a cartpole when run on CPU.

minor increase in precision does not reflect in the control values, thus saturating the performance. Also, for the intercepts spaced linearly and from a uniform distribution, there is a minimum around 0.3. This is because with larger intercepts, more neurons fire only for the higher inputs, and the precision for lower values of control decreases. This is not observed in the normal distribution as most intercepts are concentrated around the mean (0). These results are visually apparent from Figures 16.

It is also seen that the control effort is very high for low values of intercept where all neurons fire for the entire range of inputs, as compared to the case where the intercepts are more distributed over a wide range.

However, there is no pronounced effect of firing rate on the error or effort metrics.

Table 10: Performance Metrics for linearly spaced intercepts with a varying range

Range	Ts (s)	Tr (s)	PO (%)	SSE (%) $\times 10^{-3}$	IAE (rad.s) $\times 10^{-3}$	ITAE (rad.s ²) $\times 10^{-3}$	ISC (N ² .s) $\times 10^2$
-1.0 to 1.0	5.181	0.814	-25.491	2.200	207.132	321.833	2.044
-0.75 to 0.75	5.130	0.815	-25.516	-1.670	206.592	318.035	2.029
-0.5 to 0.5	5.149	0.816	-25.348	-0.634	204.111	313.622	2.034
-0.25 to 0.25	4.725	0.819	-28.664	-0.250	201.531	287.758	2.111
-0.1 to 0.1	6.065	0.847	-17.316	-92.0	197.172	365.274	3.616

Table 11: Performance Metrics for intercepts sampled from a normal distribution centred at 0 with varying standard deviations.

STD	Ts (s)	Tr (s)	PO (%)	SSE (%) $\times 10^{-3}$	IAE (rad.s) $\times 10^{-3}$	ITAE (rad.s ²) $\times 10^{-3}$	ISC (N ² .s) $\times 10^2$
0.0	6.081	0.848	-17.215	-85.7	197.437	367.653	3.671
0.1	5.318	0.806	-27.390	-3.280	213.380	341.667	2.176
0.2	5.276	0.815	-24.272	1.190	205.378	326.067	2.031
0.3	5.002	0.818	-26.016	-0.453	204.000	312.081	2.019
0.4	5.141	0.816	-25.142	-0.334	204.259	313.208	2.0166

Table 12: Performance Metrics for intercepts sampled from a uniform distribution with a varying range.

Range	Ts (s)	Tr (s)	PO (%)	SSE (%) $\times 10^{-3}$	IAE (rad.s) $\times 10^{-3}$	ITAE (rad.s ²) $\times 10^{-3}$	ISC (N ² .s) $\times 10^2$
-1.0 to 1.0	5.077	0.817	-25.803	-1.560	203.601	307.952	2.053
-0.75 to 0.75	5.176	0.817	-26.4210	-0.299	208.375	321.426	2.020
-0.5 to 0.5	5.115	0.822	-24.724	0.443	201.103	306.424	2.029
-0.25 to 0.25	4.443	0.819	-30.902	-1.400	205.643	284.705	2.151
-0.1 to 0.1	5.420	0.816	-28.106	254.0	229.290	391.814	2.244

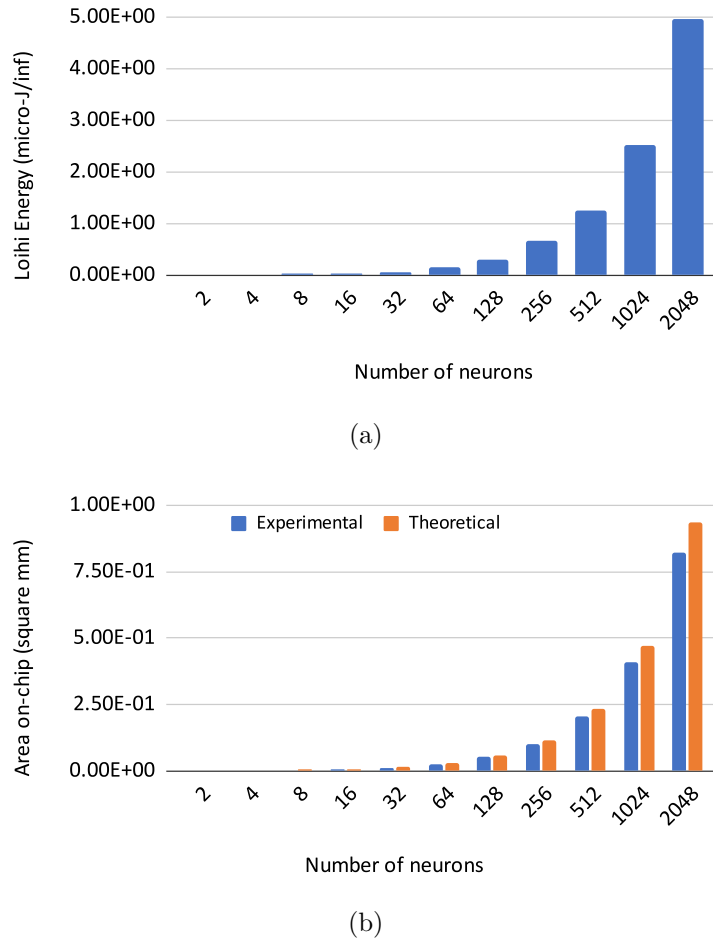


Figure 14: Change of (a) energy consumption and (b) chip area with the number of neurons for a cartpole.

The time metrics are seen to increase with a decrease in firing rate, because the higher the firing rate, the higher is the precision of control, and faster is the convergence.

Ensemble of LIF neurons for the feedback control of a higher DOF mechanical system The plots for experiments in Table 4 are shown in Figure 17 and Figure 18. The angles of the links with respect to the UEP, in the multi-linked pendulum scenario are chosen to be different to avoid loss of generality. Although, theoretically, an under-actuated multi-linked pendulum has full linear controllability, the following conditions were used to choose the angles of the links with respect to the UEP:

- (i) $\theta_1 = 0.2^c \approx 11.46^\circ$
- (ii) $\theta_n = \theta_1 - 0.02^\circ \times (n - 1)$

where, θ_1 is the angle of the link directly attached to the cart and θ_n is the n^{th} link from the cart.

In the Lagrangian equations, for the general case (see Equation 15) there are $(\theta_i - \theta_j)$

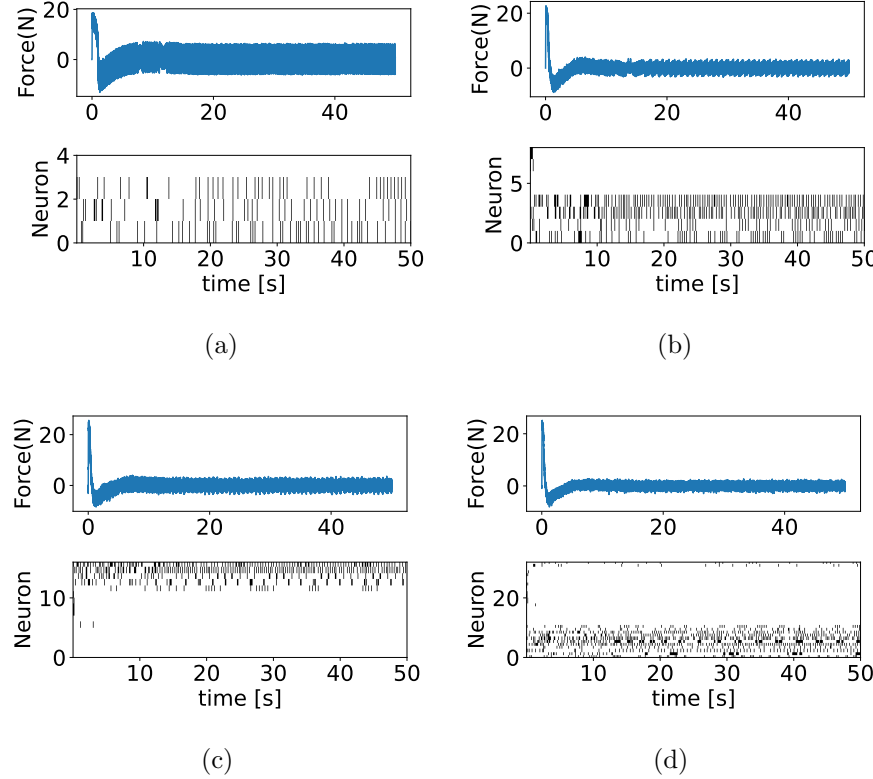


Figure 15: Control signal profile and spike raster plots for balancing a cartpole using a Nengo ensemble with (a) 4, (b) 8, (c) 16, and (d) 32 neurons respectively.

Table 13: Performance Metrics for Different Ranges of maximum firing rates

Limits	Ts (s)	Tr (s)	PO (%)	SSE $\times 10^{-3}$	IAE $(rad.s)$ $\times 10^{-3}$	ITAE $(rad.s^2)$ $\times 10^{-3}$	ISC $(N^2.s)$ $\times 10^2$
200 to 400	5.093	0.817	-25.696	1.180	205.886	314.376	2.029
250 to 400	5.050	0.822	-25.833	-0.961	203.182	305.407	2.021
300 to 400	5.159	0.814	-25.121	-0.216	205.321	317.080	2.018
350 to 400	5.080	0.816	-25.744	1.430	204.742	310.726	2.019
400 to 400	5.146	0.816	-25.484	0.075	205.110	314.930	2.014
200 to 300	5.136	0.814	-25.392	1.140	206.634	319.050	2.061
250 to 300	5.160	0.817	-25.882	-4.850	206.187	315.121	2.032
300 to 300	5.146	0.815	-25.927	2.300	207.626	320.225	2.048
200 to 200	5.234	0.825	-23.774	0.854	202.276	315.596	2.066

terms present along with the dot products of angles. In the linearity assumption, these terms are neglected, so the angles are to be chosen carefully so that the time derivatives and angle differences are not too large. Table 14 shows the control performance metrics

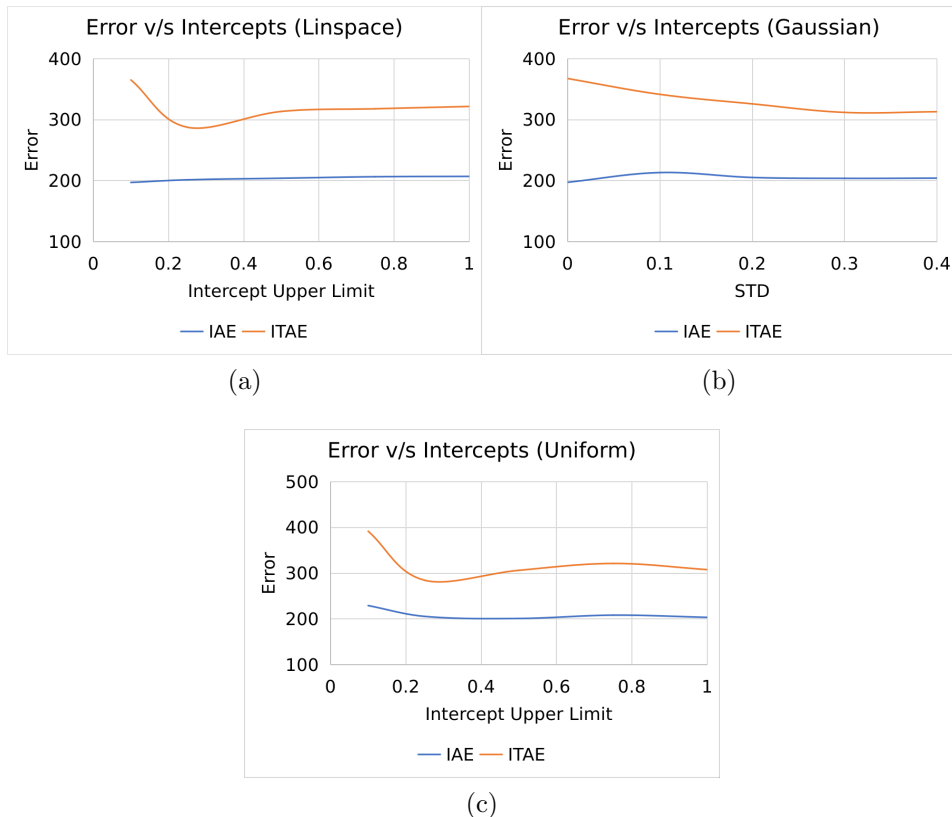


Figure 16: Variation of IAE and ITAE with (a) Range of linearly sampled intercepts about 0, (b) Standard deviation of intercepts sampled from a normal distribution centred at 0, (c) Range of intercepts sampled from a uniform distribution. The y-axis shows errors scaled by 10^3 .

for this set of experiments.

The overshoot for a particular link is seen to be proportional to the starting angle of the link, as expected. Moreover, the time metrics and the steady state error of all the links are roughly the same. A slight increase in time metrics is observed as the number of links is increased, which is obvious, since with more un-actuated DOFs, the control becomes more difficult.

4.2.2. Hardware This subsection outlines the results of implementing control of a multi-linked pendulum on a cart system using spiking neurons implemented on Intel’s Loihi neuromorphic hardware. Figure 19 shows the state evolution, phase portrait, and spike raster plots for a cartpole and a double pendulum on a cart system. Table 15 shows the transient and steady-state metrics for the experiments with Loihi. The following observations emerge from the results shown:

- (i) Overall, the performance metrics for on-chip implementation is slightly poorer than the simulation. This is because noise levels on the chip are much more than the simulation.

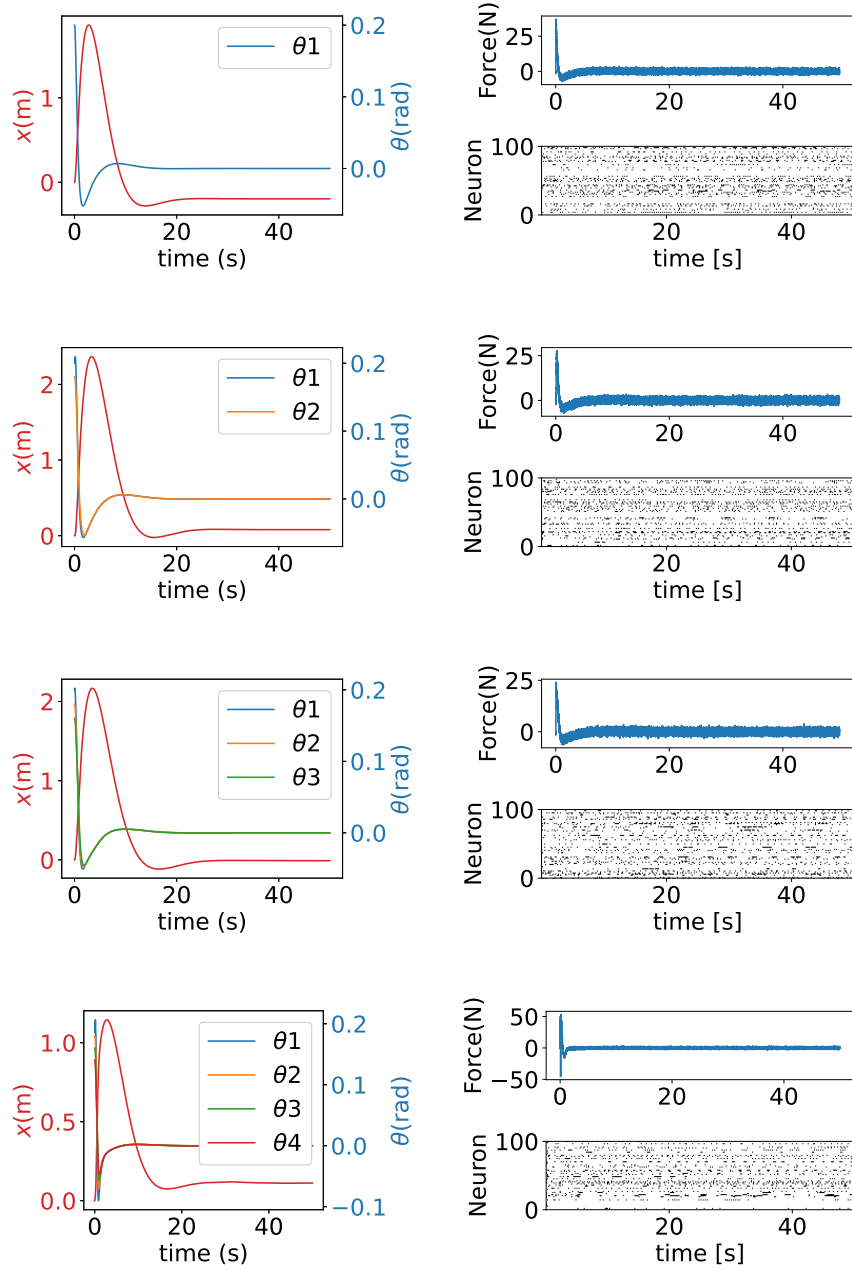


Figure 17: Plots for multi-linked pendulum on a cart system. The left column shows the evolution of $\theta(s)$ and x , and the right column shows the control force profile and spike raster plot. From top to bottom, the figures show the curves for a cartpole, a double pendulum on a cart, a triple pendulum on a cart, and a four-linked pendulum on a cart.

- (ii) The links with a higher starting angle have more overshoot as expected.
- (iii) Control fails for triple, and 4-linked pendulum on a cart, i.e., the poles fall over and are not balanced on the cart for these systems. Clearly, the bounds of accuracy that Loihi provides do not cater to the precision of control demanded by these

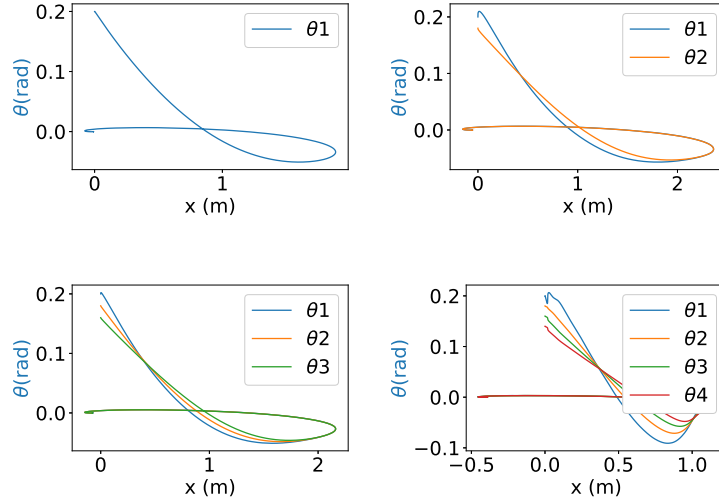


Figure 18: Phase portraits of pole angle versus cart position for multi-linked pendulum on a cart system. (a), (b), (c) and (d) illustrate the phase portraits for a cartpole, a double-linked, triple-linked and 4-linked pendulum on a cart, respectively.

Table 14: LQR control performance metrics for Nengo neural ensemble-based control of the cartpole system across varying number of links.

Metrics	Cartpole	DPC		3lPC			4lPC			
	θ	θ_1	θ_2	θ_1	θ_2	θ_3	θ_1	θ_2	θ_3	θ_4
Rise time (s)	0.813		0.976		1.057			0.765		
PO (%)	0.255		0.28	0.26	0.245	0.230	0.220	0.415	0.315	0.26
Settling time (s)	16.747		18.130		22.44			22.01		0.22
SSE	0.0005		0.0006		0.0005			0.0006		

Table 15: LQR control performance metrics for Nengo neural ensemble-based control of the cartpole system across varying number of links on Loihi.

Metrics	Cartpole	DPC	
	θ	θ_1	θ_2
Rise time (s)	0.858		0.810
PO (%)	0.255		0.57 0.368
Settling time (s)	18.552		20.455
SSE	0.0005		0.0003

under-actuated higher-DOF cartpole systems.

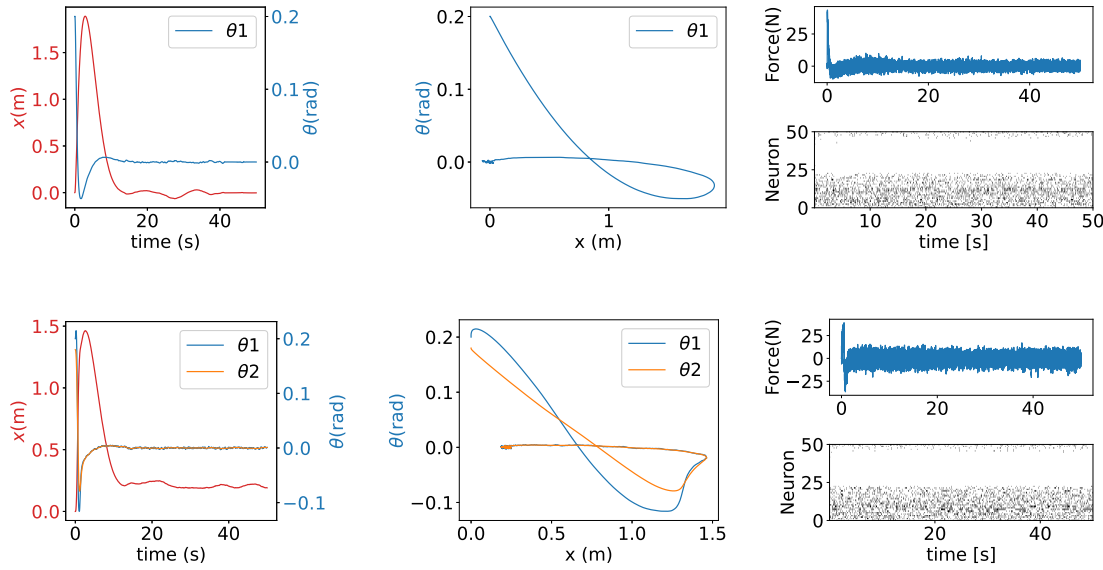


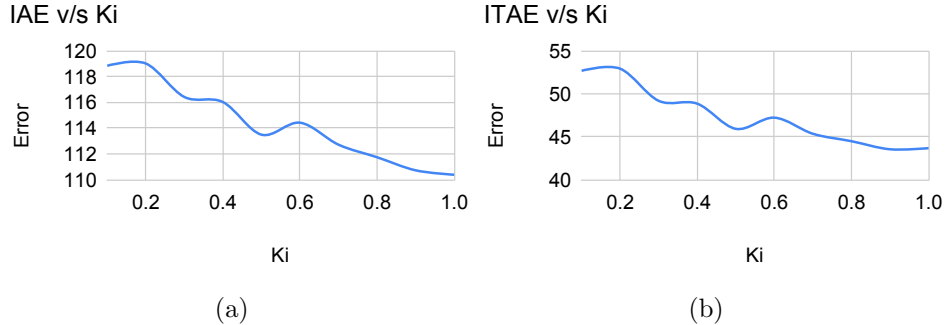
Figure 19: Plots for control multi-linked pendulum on a cart system. The left column shows the evolution of $\theta(s)$ and x , the middle column shows the phase portrait of $\theta(s)$ versus x , and the right column shows the control force profile and spike raster plot. From top to bottom, the figures show the curves for a cartpole and a double pendulum on a cart.

4.2.3. Comparison with other Models of Control This section demonstrates a comparison of the spiking LQR performance metrics with spiking PID, both using 100 spiking neurons. The main drawback of LQR is that the K_p , K_i , and K_d coefficients should be tuned to match the control metrics desired for the system, based on certain heuristics. However for optimal control methods like LQR, one can specify state and control costs (Q and R matrices), and solve the algebraic Riccati equation to get the desired value of the feedback coefficients. To establish a fair comparison, the K_p and K_d values are chosen to match the corresponding LQR coefficients for the pole angle and pole angular velocity, and then the K_i value is progressively increased from 0 to 1 to see the effect of adding the integral controller to the PD controller. Here, K_p is fixed at 190.61 and K_d is chosen to be 78.26. The case of $K_i = 0$ corresponds to the case of LQR pole angle control. Table 16 summarises the 7 performance metrics of control across varying K_i .

It is observed that the error metrics decrease and the response becomes faster (seen as a decrease in the rise and peak time), with an increase in the value of K_i (See Figure 20. However, to achieve faster control, the response overshoots. Hence, the overshoot increases with an increase in K_i . Overall, it is seen, that if the K_p and K_d values can be tuned to match the performance of an LQR controller, adding the integral control improves performance. However, the challenge of fine-tuning a PID controller as per the desired response makes LQR a better choice for linear optimal control.

Table 16: Performance Metrics for Different Values of K_i in PID control of the pole angle of a cartpole.

K_i	PO (%)	Tr (s)	Ts (s)	SSE $\times 10^{-3}$	IAE $(rad.s) \times 10^{-3}$	ITAE $(rad.s^2) \times 10^{-3}$	ISC $(N^2.m^2.s) \times 10^2$
0.0	0.0	0.0	10.0	0.710	121.813	56.698	1.505
0.1	0.0	0.0	10.0	0.041	118.855	52.695	1.509
0.2	0.0	0.0	10.0	0.191	119.033	52.945	1.514
0.3	-0.531	2.174	2.177	-0.749	116.432	49.198	1.524
0.4	-0.559	2.133	2.174	-0.462	116.038	48.866	1.527
0.5	-1.328	1.840	2.112	-0.982	113.502	45.933	1.533
0.6	-0.908	2.019	2.147	-1.115	114.432	47.233	1.539
0.7	-1.351	1.808	2.102	-1.568	112.723	45.357	1.538
0.8	-2.399	1.617	2.050	-1.982	111.746	44.489	1.545
0.9	-1.974	1.636	2.044	-1.002	110.730	43.550	1.558
1.0	-3.743	1.472	1.990	-3.885	110.387	43.681	1.558

Figure 20: Variation of (a) IAE and (b) ITAE with k_i for the spiking PID control of the pole angle of a cartpole.

A detailed comparison with different models of control are highlighted in Table 17. The errors are scaled by 10^3 .

4 spiking and 4 non-spiking control models are compared and contrasted. Between spiking LQR and spiking adaptive LQR control, it is seen that adding the adaptive block decreases the time of convergence, which is evident from the Tr metric. The integral error metrics IAE and ITAE are also seen to decrease on adding the adaptive control block. However, due to faster convergence, the spiking adaptive controller causes the response to overshoot more than the spiking LQR controller working alone. A comparison between spiking PID and spiking LQR shows that spiking PID shows lesser overshoot and a quicker response compared to LQR control, which is expected since adding an integral block to the controller keeping the proportional and derivative

Table 17: Comparison of control methods for spiking and non-spiking models. In all these examples, both the position of the cart and the angle of the pole are being controlled.

	Controller	PO (%)	Tr (s)	Ts (s)	SSE ($\times 10^{-3}$)	IAE ($\text{rad} \cdot \text{s}$)	ITAE ($\text{rad} \cdot \text{s}^2$)	ISC ($N^2 \cdot m^2 \cdot s$)
Spiking	LQR	-26.57	0.814	5.008	$1.39E-4$	205.663	305.787	2.09
	Adaptive LQR	-31.89	0.599	5.081	$-2.00E-2$	166.678	218.951	0.431
	PID	-24.61	0.681	5.268	$-1.22E-2$	205.976	320.914	2.07
	Neural imitator	-52.60	0.832	5.67	-37.5	349.365	528.552	7.65
Non-spiking	LQR	$-9.61E-3$	0.100	5.122	$2.90E-6$	203.216	313.462	1.87
	PID	$-7.12E-2$	0.100	5.276	$-9.05E-3$	210.399	334.977	1.95
	MPC	-10.2	0.100	1.511	11.1	66.236	16.474	3.23
	SMC	$-5.41E-4$	0.002	0.800	$4.59E-4$	$9.05E-4$	$3.61E-4$	7.20

coefficients same as the LQR controller, causes the PID controller to be more sensitive to the integral errors, and settle down faster. However, the ITAE metric is around 5% higher for PID, although the IAE metric is comparable. This is possibly because with an increase in time, the decrease in the steady-state error becomes less for PID controller, as compared to an LQR controller. The non-spiking LQR and PID controllers show a similar trend, but the transient and steady-state metrics are much better for the non-spiking case, as compared to the spiking scenario. This is expected, since a neuromorphic controller is less precise in its outputs, compared to a non-spiking analog controller. The SMC (Sliding Mode Controller) applies "bang-bang" type control, so the controller is faster than LQR or PID, as is seen from the Tr and Ts metrics. Also, the peak overshoot is 1 order of magnitude lower than LQR, and the steady-state-error is comparable with LQR. Even the IAE and ITAE are 6 orders of magnitude lower compared to the LQR and PID controllers. This is because the control force for SMC is high (as seen from the control effort metric), allowing for a quick decrease in the error values. MPC optimizes the trajectory of the controller till a certain time in the future, at every time step. Hence, due to progressive optimizations, the overshoot and steady-state errors are much higher compared to LQR controller, since at every time step, the optimizer detects that value of the pole angle and tries to bring it close to the target angle. The spiking neural imitator, based on the PES learning rule, trains a neural network using supervised learning, with the output from a standard spiking LQR controller as the target control value. As expected in learning-based control, the error and time metrics are worse compared to the spiking classical controllers. The control effort for neural imitator is seen to be about 3 times higher than the spiking LQR controller. Despite poorer metrics, the strength of a learning-based controller lies in its ability to adapt to changes in system parameters and environmental conditions, and to control a system solely from its input-output data, without requiring accurate knowledge of the system dynamics.

A list of neuromorphic metrics for these models of control are listed in Table 18. No improvements in computational performance metrics are seen when a neuromorphic

Table 18: Neuromorphic metrics for different models of control on CPU.

	Controller	Sim time (s)	Wall time (s)	Real time factor	Max memory RSS (MiB)	Peak allocated (MiB)	Spikes/neuron ($\times 10^5$)	Estimated CPU energy (J)
Spiking	LQR	10	19.597	0.510	1561.621	323.871	8.674	7.829
	PID	10	22.999	0.435	320.676	19.839	8.705	5.376
	Adaptive	10	22.227	0.449	896.492	29.807	8.684	7.179
	Neural Imitator	10	25.138	0.398	386.996	19.764	1.743	9.534
Non-spiking	PID	10	19.278	0.519	897.164	3.417	-	3.858
	LQR	10	18.217	0.549	317.253	2.264	-	6.927
	SMC	10	14.937	0.669	922.816	2.089	-	5.796
	MPC	10	1200.048	0.009	317.429	7.907	-	495.824

algorithm is being run on a CPU, which is a non-neuromorphic hardware. However, based on evidences in literature[10], a substantial decrease in energy consumption and latency is expected when this is run on neuromorphic hardware such as Loihi or SpiNNaker.

5. Conclusions

A linear controller for the stabilization of a cartpole has been demonstrated using simulated LIF neurons and actual hardware. From the nature of control, it is clear that 2 neurons (for end-to-end control) can be the lowest number of neurons necessary for such control, but in order to achieve precise control with good performance, a collection(ensemble) of neurons would be needed. Nengo is chosen as the framework for deploying an ensemble of neurons. It is seen that with 2 neurons in the ensemble, the tuning curves show a rate-encoding behavior, but on increasing the number of neurons in the ensemble, the control accuracy increases, since each neuron encodes a part of the input signal. Taking an appropriate population for the ensemble, simulations were done using Nengo, for pendulum on a cart systems with varying number of links. This work also demonstrates, through the chosen classic cartpole control example, how two different encoding schemes have different effects on the control performance. To this effect, a rate and a population-based encoding scheme have been presented and the effects on the KPIs of control and neuromorphic are shown. The following observations emerge from this study:

- (i) Although the control performance saturates after about 100 neurons, the CPU memory allocation and Loihi’s percentage core utilization keep increasing with the number of neurons. Hence, to operate within the bounds of power and on-board resources, limiting the number of neurons is essential.
- (ii) Rate-based encoding is a good option if there are strict constraints on the number of spiking neurons and hence, the power and on-board area utilization. While rate-encoding is robust and can achieve control with very few neurons (2 in our case), it has larger inference times and lesser precision.

- (iii) Population encoded neurons provide a higher precision for control but at the cost of a higher number of neurons and synapses, which imply higher resource on-board and higher power consumption.
- (iv) It is seen that for a 128 neuron ensemble, Loihi consumes 3 orders of magnitude less power than CPU, which decreases all the way to 5 orders of magnitude for a 2 neuron ensemble.
- (v) The fact that the same collection of neurons, (100 in this study) could perform balancing of a pendulum across so many experiments indicates that a range of DOF variation for the inverted pendulum systems can be handled with a constant number of neurons to reduce overhead for spiking neural processors.
- (vi) Although possible in Nengo simulation, the precision and noise levels in Intel's Loihi neuromorphic board do not allow for linear control of more than 2-linked pendulum on a cart, for the chosen set of control, system and neuron parameters.
- (vii) The performance metrics for different models of control indicate that LQR is a better choice for linear control over PID, when the exact coefficients for the states and their derivatives are to be determined based on the desired control performance. However, once these coefficients are known, adding an integral block improves the time and error metrics.
- (viii) The spiking version of these controllers shows poorer performance compared to the non-spiking ones, which is expected due to higher noise levels and lower precision of spiking networks. However, the spiking controllers are expected to consume orders of magnitude less power and compute at a much lower latency, when run on neuromorphic hardware.
- (ix) Although training a spiking neural network for such control increases the time to converge and the error values, learning-based control is highly favoured. This is because of its adaptability to perturbations and system parameter variations, and the ability to learn the control behaviour from data, without the need for an exact model of the system.

This work can be extended to other control methodologies such as constrained LQR, where one can specify constraints on the state variables which would be important, for example, for physical cartpole systems where the length of the rails inherently limits the movement of the cart. Secondly, a linear control of these systems with the desired steady-state and transient response can be performed to check for the number of neurons needed versus the performance of control.

Acknowledgments

This publication has emanated from research conducted with the financial support of Research Ireland under Grant number 18/CRT/6049. This work was inspired by activities started at the CapoCaccia Workshop toward Neuromorphic Intelligence 2023 [22], Sardinia, Italy. The majority of the experiments were done in this lab

set up in the workshop where several researchers gathered to discuss neuromorphic problems. We would like to especially thank Sebastian Billaudelle and Yannik Stradmann from Heidelberg University, Germany for their help and support with the Lu.i board its use in our experiments. Thanks to Felix Schmitt for help with Lu.i interfacing and related linear control of cartpole, Samia Mohinta for helping us brainstorm ideas, and Tobi Delbruck from INI labs, University of Zurich for bringing a cartpole system to the workshop for implementing various algorithms. Shreyan Banerjee would like to acknowledge Rohit Chawla, for help with Digilent software and hardware. The authors would also like to acknowledge Chiara Bartolozzi from the Italian Institute of Technology for her constant support in this work. Vikram Pakrashi acknowledges Science Foundation Ireland NexSYs 21/SPP/3756, TRaIN 22/NCF/FD/10995, Harmoni 22/FFP-P/11457 and Sustainable Energy Authority of Ireland REMOTEWIND RDD/613, TwinFarm RDD/604, FlowDyn RDD/966, and Interreg SiSDATA EAPA-0040/2022.

Supplementary materials

5.1. Control Performance Metrics

This section describes the metrics of control studied in this work.

- **Rise Time (t_r):**

The time required for the system response to rise from 10% to 90% of its final steady-state value.

$$t_r = t_{90\%} - t_{10\%}$$

- **Peak Overshoot (M_p):**

The maximum overshoot relative to the steady-state value, expressed as a percentage.

$$M_p = \left(\frac{y_{\text{peak}} - y_{\infty}}{y_{\infty}} \right) \times 100\%$$

- **Settling Time (t_s):**

The time required for the output to remain within a specified tolerance band (typically $\pm 2\%$ or $\pm 5\%$) around the steady-state value.

$$t_s = \text{time when } |y(t) - y_{\infty}| < \epsilon \text{ for all } t \geq t_s$$

- **Steady-State Error (e_{ss}):**

The difference between the desired output and the actual output as time approaches infinity.

$$e_{ss} = \lim_{t \rightarrow \infty} |r(t) - y(t)|$$

- **Integral of Absolute Error (IAE):**

Measures the total absolute error over time.

$$\text{IAE} = \int_0^{\infty} |e(t)| dt$$

- **Integral of Time-weighted Absolute Error (ITAE):**

Penalizes errors that persist over time by weighting them with time.

$$\text{ITAE} = \int_0^{\infty} t \cdot |e(t)| dt$$

- **Integral of Squared Control (ISC):**

Measures the total squared control effort applied over time. Useful in penalizing aggressive control inputs.

$$\text{ISC} = \int_0^{\infty} u^2(t) dt$$

5.2. Simulation Performance Metrics

This section includes the metrics of simulation performance studied in this work.

- **Sim Time:**

The total simulated duration of the model or system, typically measured in seconds.

Example: Simulating 10 seconds of robot behavior.

- **Wall Time:**

The actual elapsed (real-world) time required to run the simulation on a computer.

Example: A 10s simulation takes 20s of wall time.

- **Real-Time Factor (RTF):**

The ratio of simulated time to wall-clock time. Indicates simulation speed relative to real time.

$$\text{RTF} = \frac{\text{Sim Time}}{\text{Wall Time}}$$

- RTF > 1: faster than real-time - RTF < 1: slower than real-time

- **Max Memory RSS (Resident Set Size):**

The maximum amount of physical RAM occupied by the simulation process during its execution, including code, data, and shared libraries.

Typically measured in mebibytes (MiB) or gibibytes (GiB).

- **Peak Allocated Memory:**

The highest amount of memory dynamically allocated by the simulation, excluding shared libraries or OS overhead.

This is often reported by memory profilers.

- **Estimated CPU Energy:**

An estimate of the total CPU energy consumed during simulation, often measured in joules (J) or watt-hours (Wh).

It is measured using the following formula:

$\text{Energy (J)} = \text{Wall Time (s)} \times \text{CPU Utilization} \times \text{TDP (W)}$, where TDP stands for the Thermal Design Power of the CPU. Useful for evaluating power efficiency, especially on embedded or neuromorphic systems.

5.3. Neuromorphic Performance Metrics

This section includes the metrics of neuromorphic performance studied in this work.

- **Spikes per neuron:**

This metric shows the average number of spikes emitted by each neuron in the network/ensemble during the simulation.

- **Core Utilization:**

This metric demonstrates the percentage of each neuromorphic core on average, utilized during building the spiking neural network model on a neuromorphic chip.

- **Experimental Area on Chip:**

This is the experimentally determined chip area allocated to the spiking neural network during simulation. It is measured using the following formula:

$$\text{Expt Area (mm}^2\text{)} = \text{Area per Core (mm}^2\text{)} \times \% \text{ per Core} \times \text{Number of Cores}$$

- **Theoretical Area on Chip:**

This is the area on chip allocated to the spiking neural network, theoretically calculated using the datasheet for the chip using the formula:

$$\text{Theo Area (mm}^2\text{)} = \frac{\text{Number of neurons in the network}}{\text{Neuron density (mm}^{-2}\text{)}}$$

- **Estimated Energy:**

This is an estimate of the energy consumed by the board (excluding the idle power consumption required to keep the board ON), calculated using the following formula:

$$\text{Energy (J/inf)} = \text{Energy/synaptic op} \times \text{synaptic ops/inf (J/inf)} + \text{Energy/neuron update} \times \text{neuron updates/inf (J/inf)}$$

5.4. Control Videos

Videos of the control in action with the spiking neurons can be seen at the following github page: <https://github.com/shreyanban/NCE Reviewed Videos>.

References

- [1] Reza Ahmadvand, Sarah Safura Sharif, and Yaser Mike Banad. A cloud-edge framework for energy-efficient event-driven control: an integration of online supervised learning, spiking neural networks and local plasticity rules. *Neuromorphic Computing and Engineering*, 4(4):044004, 2024.
- [2] Diego Chavez Arana, Luis Rodolfo Garcia Carrillo, Ignacio Rubio Scola, Eduardo S Espinoza, Andrew T Sornborger, et al. Spiking neural network-based flight controller. In *2024 Neuro Inspired Computational Elements Conference (NICE)*, pages 1–8. IEEE, 2024.
- [3] Diego Chavez Arana, Eduardo S Espinoza, Luis Rodolfo García Carrillo, Antonio Osorio Cordero, Andrew T Sornborger, et al. Spiking neural network-based control applied to an underactuated system. In *2023 20th International Conference on Electrical Engineering, Computing Science and Automatic Control (CCE)*, pages 1–6. IEEE, 2023.
- [4] Shreyan Banerjee, Aasifa Rounak, and Vikram Pakrashi. Adaptive linear control of a cartpole using minimum spiking neurons trained with prescribed error sensitivity. In *2024 21st International Conference on Mechatronics-Mechatronika (ME)*, pages 1–9. IEEE, 2024.
- [5] Shreyan Banerjee, Aasifa Rounak, and Vikram Pakrashi. Control of an under-actuated cartpole with an evolving neural topology using synaptic bellman equation. In *2024 13th International Conference on Modern Circuits and Systems Technologies (MOCAST)*, pages 01–04. IEEE, 2024.
- [6] Trevor Bekolay, James Bergstra, Eric Hunsberger, Travis DeWolf, Terrence Stewart, Daniel Rasmussen, Xuan Choo, Aaron Voelker, and Chris Eliasmith. Nengo: a python tool for building large-scale functional brain models. *Frontiers in Neuroinformatics*, 7, 2014.
- [7] Trevor Bekolay, James Bergstra, Eric Hunsberger, Travis DeWolf, Terrence C Stewart, Daniel Rasmussen, Xuan Choo, Aaron Russell Voelker, and Chris Eliasmith. Nengo: a python tool for building large-scale functional brain models. *Frontiers in neuroinformatics*, 7:48, 2014.
- [8] bertozzijr. Control bootcamp s brunton, 2018.
- [9] Matthew Cook. It takes two neurons to ride a bicycle. *Demonstration at NIPS*, 4, 2004.

- [10] Mike Davies, Narayan Srinivasa, Tsung-Han Lin, Gautham Chinya, Yongqiang Cao, Sri Harsha Choday, Georgios Dimou, Prasad Joshi, Nabil Imam, Shweta Jain, et al. Loihi: A neuromorphic manycore processor with on-chip learning. *Ieee Micro*, 38(1):82–99, 2018.
- [11] Travis DeWolf, Paweł Jaworski, and Chris Eliasmith. Nengo and low-power ai hardware for robust, embedded neurorobotics. *Frontiers in Neurorobotics*, 14:568359, 2020.
- [12] Travis DeWolf, Kinjal Patel, Paweł Jaworski, Roxana Leontie, Joe Hays, and Chris Eliasmith. Neuromorphic control of a simulated 7-dof arm using loihi. *Neuromorphic Computing and Engineering*, 3(1):014007, 2023.
- [13] Travis DeWolf, Terrence C Stewart, Jean-Jacques Slotine, and Chris Eliasmith. A spiking neural model of adaptive arm control. *Proceedings of the Royal Society B: Biological Sciences*, 283(1843):20162134, 2016.
- [14] Santiago Díaz-Romero, Marcin Paluch, Alejandro Linares-Barranco, and Antonio Rios-Navarro. On implementing the sparse events closed-loop control theory for the cartpolesimulation. In *International Conference on Simulation Tools and Techniques*, pages 239–254. Springer, 2024.
- [15] Digilent. Digilent: An ni company, 2023.
- [16] Michael Ehrlich, Yuval Zaidel, Patrice L Weiss, Arie Melamed Yekel, Naomi Gefen, Lazar Supic, and Elishai Ezra Tsur. Adaptive control of a wheelchair mounted robotic arm with neuromorphically integrated velocity readings and online-learning. *Frontiers in Neuroscience*, 16:1007736, 2022.
- [17] Razvan V Florian. Correct equations for the dynamics of the cart-pole system. *Center for Cognitive and Neural Studies (Coneural), Romania*, page 63, 2007.
- [18] Guillermo Gallego, Tobi Delbrück, Garrick Orchard, Chiara Bartolozzi, Brian Taba, Andrea Censi, Stefan Leutenegger, Andrew J Davison, Jörg Conradt, Kostas Daniilidis, et al. Event-based vision: A survey. *IEEE transactions on pattern analysis and machine intelligence*, 44(1):154–180, 2020.
- [19] Wulfram Gerstner, Werner M Kistler, Richard Naud, and Liam Paninski. *Neuronal dynamics: From single neurons to networks and models of cognition*. Cambridge University Press, 2014.
- [20] Ian Grout and Abu Khari bin A’ain. Introductory laboratories in semiconductor devices using the digilent analog discovery. In *Proceedings of 2015 12th International Conference on Remote Engineering and Virtual Instrumentation (REV)*, pages 1–6. IEEE, 2015.
- [21] Jingxiu He, Li Cui, Jingru Sun, Pan Huang, and Yuan Huang. Chaotic dynamics analysis of double inverted pendulum with large swing angle based on hamiltonian function. *Nonlinear Dynamics*, 108(4):4373–4384, 2022.
- [22] iniForum GmbH. The capocaccia workshops toward neuromorphic intelligence, 2014.
- [23] Maidul Islam, Mohamed Okasha, E Sulaeman, S Fatai, and Ari Legowo. Performance evaluation of linear quadratic regulator and linear quadratic gaussian controllers on quadrotor platform. *International Journal of Recent Technology and Engineering*, 7:191–195, 2019.
- [24] Eugene M Izhikevich. Simple model of spiking neurons. *IEEE Transactions on neural networks*, 14(6):1569–1572, 2003.
- [25] Jorge A Juárez-Lora, Juan Humberto Sossa Azuela, Víctor Hugo Ponce Ponce, Elsa Rubio-Espino, and Ricardo Barrón Fernández. Spiking neural network implementation of lqr control on underactuated system. *Int. J. Comb. Optim. Probl. Informatics*, 13(4):36–46, 2022.
- [26] Kadierdan Kaheman, Urban Fasel, Jason J Bramburger, Benjamin Strom, J Nathan Kutz, and Steven L Brunton. The experimental multi-arm pendulum on a cart: A benchmark system for chaos, learning, and control. *HardwareX*, 15:e00465, 2023.
- [27] Dailin Marrero, John Kern, and Claudio Urrea. A novel robotic controller using neural engineering framework-based spiking neural networks. *Sensors*, 24(2):491, 2024.
- [28] Mark Nelson and John Rinzel. The hodgkin-huxley model. *The book of genesis*, pages 29–49, 1995.
- [29] Norman S Nise. *Control systems engineering*. John Wiley & Sons, 2020.
- [30] K Pakdaman. Periodically forced leaky integrate-and-fire model. *Physical Review E*, 63(4):041907,

2001.

- [31] Fernando Perez-Peña, Arturo Morgado-Estevez, Alejandro Linares-Barranco, Angel Jimenez-Fernandez, Francisco Gomez-Rodriguez, Gabriel Jimenez-Moreno, and Juan Lopez-Coronado. Neuro-inspired spike-based motion: From dynamic vision sensor to robot motor open-loop control through spike-vite. *Sensors*, 13(11):15805–15832, 2013.
- [32] James S Plank, Charles P Rizzo, Chris A White, and Catherine D Schuman. The cart-pole application as a benchmark for neuromorphic computing. *Journal of Low Power Electronics & Applications*, 15(1), 2025.
- [33] Cosmin Popa. Improved accuracy current-mode multiplier circuits with applications in analog signal processing. *IEEE transactions on very large scale integration (VLSI) systems*, 22(2):443–447, 2013.
- [34] Huanneng Qiu, Matthew Garratt, David Howard, and Sreenatha Anavatti. Evolving spiking neural networks for nonlinear control problems. In *2018 IEEE Symposium Series on Computational Intelligence (SSCI)*, pages 1367–1373. IEEE, 2018.
- [35] Andrew W Rafe, Jaime A Garcia, and William L Raffe. Exploration of encoding and decoding methods for spiking neural networks on the cart pole and lunar lander problems using evolutionary training. In *2021 IEEE Congress on Evolutionary Computation (CEC)*, pages 498–505. IEEE, 2021.
- [36] Justin B Rowe, Vicky Chan, Morgan L Ingemanson, Steven C Cramer, Eric T Wolbrecht, and David J Reinkensmeyer. Robotic assistance for training finger movement using a hebbian model: a randomized controlled trial. *Neurorehabilitation and neural repair*, 31(8):769–780, 2017.
- [37] Prathamesh Saraf, Manan Gupta, and Alivelu Manga Parimi. A comparative study between a classical and optimal controller for a quadrotor. In *2020 IEEE 17th India Council International Conference (INDICON)*, pages 1–6. IEEE, 2020.
- [38] Filip S Slijkhuis, Sander W Keemink, and Pablo Lanillos. Closed-form control with spike coding networks. *IEEE Transactions on Cognitive and Developmental Systems*, 2023.
- [39] Rasmus Stagsted, Antonio Vitale, Jonas Binz, Leon Bonde Larsen, and Yulia Sandamirskaya. Towards neuromorphic control: A spiking neural network based pid controller for uav. RSS, 2020.
- [40] Yannik Stradmann, Julian Göltz, Mihai A Petrovici, Johannes Schemmel, and Sebastian Billaudelle. Lu. i—a low-cost electronic neuron for education and outreach, 2025.
- [41] Federico Paredes Valles, Jesse Hagenaars, Julien Dupeyroux, Stein Stroobants, Yingfu Xu, and Guido de Croon. Fully neuromorphic vision and control for autonomous drone flight. *arXiv*, 2023.
- [42] Lan-Da Van, Shuenn-Shyang Wang, and Wu-Shiung Feng. Design of the lower error fixed-width multiplier and its application. *IEEE Transactions on Circuits and Systems II: Analog and Digital Signal Processing*, 47(10):1112–1118, 2000.
- [43] Alex Volinski, Yuval Zaidel, Albert Shalumov, Travis DeWolf, Lazar Supic, and Elishai Ezra Tsur. Data-driven artificial and spiking neural networks for inverse kinematics in neurorobotics. *Patterns*, 3(1), 2022.
- [44] Hongliang Wang, Haobin Dong, Lianghua He, Yongle Shi, and Yuan Zhang. Design and simulation of lqr controller with the linear inverted pendulum. In *2010 International Conference on Electrical and Control Engineering*, pages 699–702, 2010.
- [45] Lukasz Wiklendt, Stephan Chalup, and Rick Middleton. A small spiking neural network with lqr control applied to the acrobot. *Neural Computing and Applications*, 18:369–375, 2009.
- [46] Xin Xin, Kanjian Zhang, and Haikun Wei. Linear strong structural controllability for an n-link inverted pendulum in a cart. In *2018 IEEE Conference on Decision and Control (CDC)*, pages 1204–1209. IEEE, 2018.
- [47] Yuval Zaidel, Albert Shalumov, Alex Volinski, Lazar Supic, and Elishai Ezra Tsur. Neuromorphic nef-based inverse kinematics and pid control. *Frontiers in neurorobotics*, 15:631159, 2021.
- [48] Jingyue Zhao, Nicoletta Risi, Marco Monforte, Chiara Bartolozzi, Giacomo Indiveri, and Elisa

Donati. Closed-loop spiking control on a neuromorphic processor implemented on the icub. *IEEE Journal on Emerging and Selected Topics in Circuits and Systems*, 10(4):546–556, 2020.